JACS
JOURNAL OF THE AMERICAN CHEMICAL SOCIETY

Article

pubs.acs.org/JACS

Mechanistic Investigation of Bis(imino)pyridine Manganese Catalyzed Carbonyl and Carboxylate Hydrosilylation

Tufan K. Mukhopadhyay,[†] Christopher L. Rock,[†] Mannkyu Hong,[‡,§] Daniel C. Ashley,[∥] Thomas L. Groy,[†] Mu-Hyun Baik,*[,‡,§] and Ryan J. Trovitch*[,†]

[†]School of Molecular Sciences, Arizona State University, Tempe, Arizona 85287, United States
[‡]Department of Chemistry, Korea Advanced Institute of Science and Technology (KAIST), Daejeon 34141, South Korea
[§]Center for Catalytic Hydrocarbon Functionalizations, Institute for Basic Science (IBS), Daejeon 34141, South Korea
[∥]Department of Chemistry, Indiana University, Bloomington, Indiana 47405, United States

Supporting Information

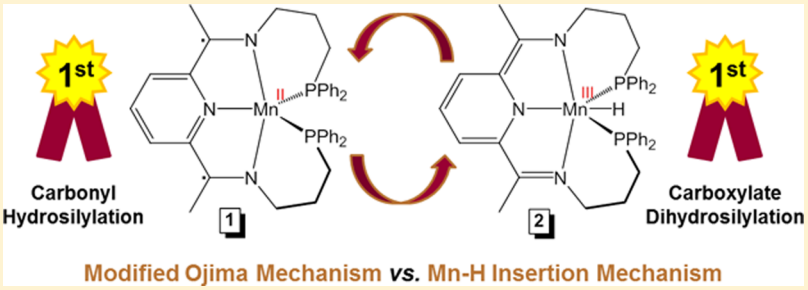

ABSTRACT: We recently reported a bis(imino)pyridine (or pyridine diimine, PDI) manganese precatalyst, (^{Ph2PPr}PDI)Mn (**1**), that is active for the hydrosilylation of ketones and dihydrosilylation of esters. In this contribution, we reveal an expanded scope for **1**-mediated hydrosilylation and propose two different mechanisms through which catalysis is achieved. Aldehyde hydrosilylation turnover frequencies (TOFs) of up to 4900 min^{-1} have been realized, the highest reported for first row metal-catalyzed carbonyl hydrosilylation. Additionally, **1** has been shown to mediate formate dihydrosilylation with leading TOFs of up to 330 min^{-1}. Under stoichiometric and catalytic conditions, addition of $PhSiH_3$ to (^{Ph2PPr}PDI)Mn was found to result in partial conversion to a new diamagnetic hydride compound. Independent preparation of (^{Ph2PPr}PDI)MnH (**2**) was achieved upon adding $NaEt_3BH$ to (^{Ph2PPr}PDI)$MnCl_2$ and single-crystal X-ray diffraction analysis revealed this complex to possess a capped trigonal bipyramidal solid-state geometry. When 2,2,2-trifluoroacetophenone was added to **1**, radical transfer yielded (^{Ph2PPr}PDI•)Mn(OC•(Ph)(CF_3)) (**3**), which undergoes intermolecular C−C bond formation to produce the respective Mn(II) dimer, [(μ-*O*,N_{py}-4-OC(CF_3)(Ph)-4-H-^{Ph2PPr}PDI)Mn]$_2$ (**4**). Upon finding **3** to be inefficient and **4** to be inactive, kinetic trials were conducted to elucidate the mechanisms of **1**- and **2**-mediated hydrosilylation. Varying the concentration of **1**, substrate, and $PhSiH_3$ revealed a first order dependence on each reagent. Furthermore, a kinetic isotope effect (KIE) of 2.2 ± 0.1 was observed for **1**-catalyzed hydrosilylation of diisopropyl ketone, while a KIE of 4.2 ± 0.6 was determined using **2**, suggesting **1** and **2** operate through different mechanisms. Although kinetic trials reveal **1** to be the more active precatalyst for carbonyl hydrosilylation, a concurrent **2**-mediated pathway is more efficient for carboxylate hydrosilylation. Considering these observations, **1**-catalyzed hydrosilylation is believed to proceed through a modified Ojima mechanism, while **2**-mediated hydrosilylation occurs via insertion.

INTRODUCTION

Hydrosilylation catalysts have long been used to mediate Si−C and Si−O bond formation in an atom-efficient fashion.[1] Since Speier's initial observation of chloroplatinic acid-catalyzed olefin hydrosilylation,[2] precious metal catalysts have been widely used for the production of silicone adhesives, rubbers, and release coatings.[3] Olefin hydrosilylation is known to proceed through the Chalk-Harrod mechanism, which features Si−H oxidative addition, alkene insertion into M-H, and reductive elimination of the respective alkylsilane.[4] A modified Chalk-Harrod mechanism featuring alkene insertion into M-SiR_3 has also been documented to account for the formation of unsaturated byproducts.[5] Conversely, Si−O formation by way of carbonyl hydrosilylation has emerged as a mild route to alcohols that can be conducted in a stereoselective manner.[6] In the presence of monohydrosilanes, precious metal catalysts including Wilkinson's catalyst[7] are believed to mediate carbonyl hydrosilylation via the Ojima mechanism (Figure 1), whereby Si−H oxidative addition, insertion into M−SiR_3, and reductive elimination yields the respective silyl ether.[8] Recent investigations have suggested that electrophilic silylene intermediates

Received: January 25, 2017
Published: March 10, 2017

DOI: 10.1021/jacs.7b00879
J. Am. Chem. Soc. 2017, 139, 4901−4915

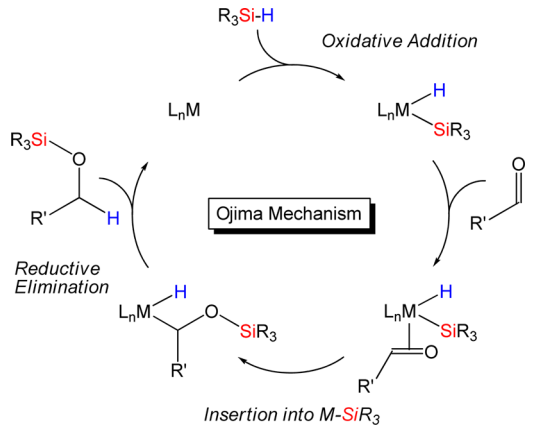

Figure 1. Ojima mechanism for carbonyl hydrosilylation.

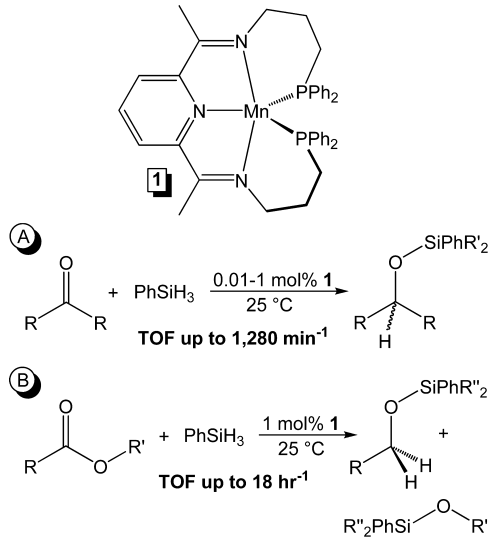

Figure 2. Ketone hydrosilylation (A) and ester dihydrosilylation (B) using **1**.[25]

are responsible for Rh-catalyzed carbonyl reduction in the presence of dihydro- and trihydrosilanes.[9] Similarly, σ-silane complexes of Ru and Ir are believed to mediate carbonyl hydrosilylation by promoting substrate nucleophilic attack at Si.[10]

Although precious metal catalyzed hydrosilylation pathways have been extensively investigated, efforts to develop low-cost first row metal hydrosilylation catalysts have only recently started to intensify.[11−16] Base metal catalysts are advantageous from a cost and toxicity perspective;[17] however, they can be difficult to study since they tend to engage in one electron reaction pathways and often adopt high-spin electronic configurations.[18] This has led to a relative dearth of mechanistic information regarding first row metal carbonyl hydrosilylation, and the catalysts which have been thoroughly studied operate through widely varied mechanisms.[19] For example, although a fair number of Mn-based hydrosilylation catalysts have been reported,[20] the mechanisms through which they operate remain poorly understood. Moreover, it is unclear whether low-valent Mn^0,[21] Mn^I,[22] and Mn^{II} catalysts[23] proceed via similar or different mechanisms relative to each other or the lone high-valent Mn catalyst that is known, (3,5-^{t}Bu$_2$-salen)MnN.[24]

In 2014, we reported that formally zerovalent (^{Ph2PPr}PDI)Mn (Figure 2, **1**) achieves ketone hydrosilylation turnover frequencies (TOFs) of up to 76 800 h^{-1} (more accurately expressed as 1280 min^{-1}) and ester dihydrosilylation TOFs of up to 18 h^{-1} under ambient conditions (Figure 2).[25] Herein, we describe an expanded scope with higher activities for **1**-mediated aldehyde and formate hydrosilylation, the identification of an in situ generated Mn−H cocatalyst, and a comprehensive kinetic analysis that suggests concurrent modified Ojima and Mn−H insertion mechanisms are responsible for catalysis. With an updated understanding of catalyst electronic structure and reactivity, the role of PDI chelate denticity and non-innocence is also discussed.

RESULTS AND DISCUSSION

Expansion of Substrate Scope. Upon evaluating the ketone and ester hydrosilylation activity of **1**, we hypothesized that higher TOFs might be achieved when screening less sterically demanding aldehyde- and formate-containing substrates. Knowing that **1** mediates efficient and exothermic ketone hydrosilylation under neat conditions using $PhSiH_3$ (other silanes afford slower conversion),[25] an equimolar solution of benzaldehyde and $PhSiH_3$ was added to 0.1 mol % **1** at 25 °C. After 2 min, the reaction was exposed to air to deactivate the catalyst and NMR spectroscopic analysis revealed complete benzaldehyde hydrosilylation (TOF = 490 min^{-1}) to a 98:2 ratio of $PhSi(OCH_2Ph)_3$:$PhSiH(OCH_2Ph)_2$. Treatment with 10% aq. NaOH allowed for the isolation of benzyl alcohol (94%, Table 1, **a**) following extraction and solvent evaporation (Figures S3 and S4 in the Supporting Information). For comparison, 13 additional aldehydes were evaluated for hydrosilylation under these conditions (**b**−**n**). Notably, *p*-fluoro, *p*-chloro, and *p*-bromobenzaldehyde were efficiently hydrosilylated after 2 min (**b**−**d**) while *p*-iodobenzaldehyde reached only 32% conversion (**e**). Although electron-withdrawing and -donating groups were found to slow the rate of **1**-catalyzed ketone hydrosilylation in benzene-d_6 solution,[25] benzaldehyde substitution does not adversely influence the hydrosilylation rate under neat conditions (**f**−**i**). Substrate conversion was also unaffected by the *N*- and *O*-heterocyclic moieties of pyridine-3-carboxaldehyde and furfural (**k**,**l**) and the alkene functionalities of 3-cyclohexene-1-carboxaldehyde and citral (**m**,**n**). Importantly, **1** was found to exhibit chemoselectivity for the hydrosilylation of aldehydes over nitro (**f**), nitrile (**g**), and alkene functionalities (**m**,**n**). Catalyst homogeneity was confirmed by conducting **1**-mediated benzaldehyde hydrosilylation in the presence of excess Hg^0, which did not affect conversion. Benzaldehyde hydrosilylation was also observed using **1** in absence of light, disfavoring the possibility of light-induced catalysis.

To determine the highest attainable TOF for **1**-catalyzed aldehyde hydrosilylation, efforts were made to further reduce the catalyst loading. Adding 0.01 mol % **1** to an equimolar solution of benzaldehyde and $PhSiH_3$ (Table 2, **a**) resulted in vigorous bubbling due to the exothermic nature of this reaction. After 2 min, the catalyst was quenched upon opening to air and NMR spectroscopic analysis revealed greater than 99% conversion to a mixture of silyl ethers, equating to a TOF of 4900 min^{-1}. The same conversion was observed upon adding a stock solution of **1** in $PhSiH_3$ to a mixture of $PhSiH_3$ and benzaldehyde. Comparable hydrosilylation activity was noted for 4-fluorobenzaldehyde, 2-naphthaldehyde, and furfural (**b**−**d**) and hydrolysis of the silyl ether products yielded the corresponding alcohols in good yield (Table 2). To determine the maximum turnover number (TON) for **1**-catalyzed

DOI: 10.1021/jacs.7b00879
J. Am. Chem. Soc. 2017, 139, 4901−4915

Table 1. Hydrosilylation of Aldehydes Using 0.1 mol % 1 and $PhSiH_3$ at 25 °C[ab]

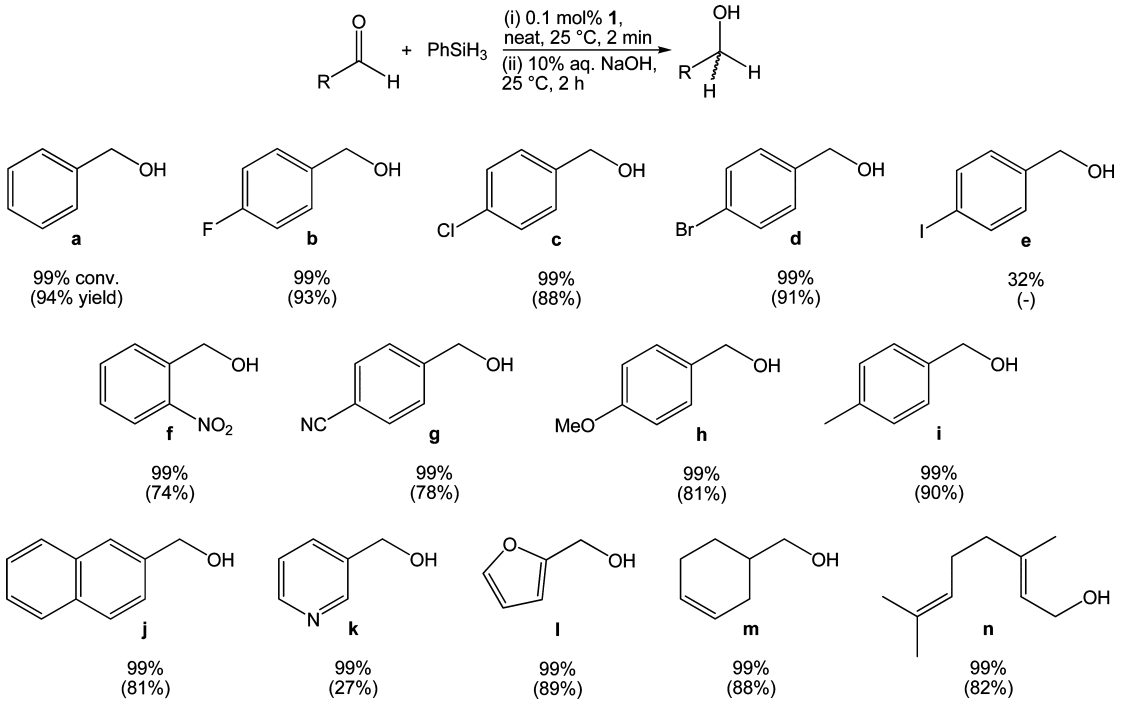

[a]Percent conversion as determined by ^{1}H NMR spectroscopy (TOF = 490 min^{-1} for all substrates except **e**). [b]Isolated yields of the corresponding alcohol in parentheses (spectroscopic analysis provided in the Supporting Information).

Table 2. Aldehyde Hydrosilylation at Low Catalyst Loading[ab]

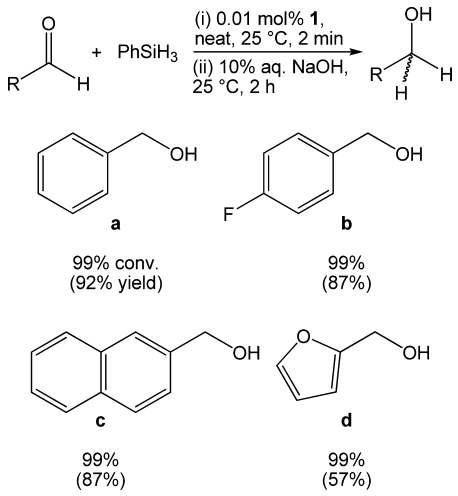

[a]Percent conversion as determined by ^{1}H NMR spectroscopy (TOF = 4900 min^{-1} for all substrates). [b]Isolated yields of the corresponding alcohol in parentheses.

aldehyde hydrosilylation, a solution containing 10 000 equiv of dry $PhSiH_3$ and benzaldehyde was added to **1**. After allowing the reaction to cool to ambient temperature for 15 min, a second solution of 10 000 equiv. $PhSiH_3$/benzaldehyde was added. This process was repeated three additional times until a total of 50 000 equiv of substrate and silane were added. Analysis of the product mixture by ^{1}H NMR spectroscopy revealed 63% overall conversion, equating to a TON of 31 000. The observed hydrosilylation TOFs are approximately 4-times higher than previously reported for **1**-mediated ketone hydrosilylation[25] and are significantly higher than those reported for leading Fe (393 min^{-1}),[12f] Co (49.5 min^{-1}),[13f] and Ni (38.4 min^{-1})[14c] carbonyl hydrosilylation catalysts.[23] The maximum TON of 31 000 is also more than double the benzaldehyde hydrosilylation TON achieved using (κ^5-*N,N,N,N,N*-^{PyEt}PDEA)Mn.[23]

Knowing that **1** catalyzes the dihydrosilylation of esters with TOFs of up to 18 h^{-1},[25] it was anticipated that a comparable activity enhancement might be observed upon investigating the dihydrosilylation of formates. When a neat equimolar mixture of either methyl or ethyl formate and $PhSiH_3$ was added to 0.02 mol % of **1**, an exothermic reaction ensued, resulting in complete conversion to a mixture of methoxy and ethoxy (in the case of ethyl formate) silyl ethers. Attempts to hydrolyze each product mixture and separate the product alcohols by fractional distillation were unsuccessful; therefore, higher molecular weight formates were chosen to allow formate dihydrosilylation optimization. Adding an equimolar quantity of benzyl formate and $PhSiH_3$ to 0.02 mol % of **1** resulted in complete substrate reduction within 15 min, and hydrolysis using 10% aq. NaOH followed by extraction and evaporation afforded pure benzyl alcohol with good yield (Table 3, **a**). Complete conversion was also observed upon adding a stock solution of **1** in $PhSiH_3$ to benzyl formate. Similarly, *p*-anisyl formate, phenylethyl formate, hexyl formate, and isoamyl formate were fully hydrosilylated using 0.02 mol % **1** over the course of 15 min and the corresponding alcohols were obtained in good-to-modest yield (**b**–**e**). For each of these transformations, **1** achieved formate dihydrosilylation with a TOF of 330 min^{-1}, orders of magnitude faster than the best known carboxylate dihydrosilylation catalysts.[26] Although citronellyl formate and geranyl formate were distilled and scrupulously dried prior to screening, it was not possible to reproducibly transform these substrates with 0.02 mol % loadings of **1**. These substrates were cleaved in 15 min to yield

DOI: 10.1021/jacs.7b00879
J. Am. Chem. Soc. 2017, 139, 4901–4915

Table 3. Hydrosilylation of Formates Using 0.02−0.1 mol % 1 or 2 and $PhSiH_3$ at 25 °C[ab]

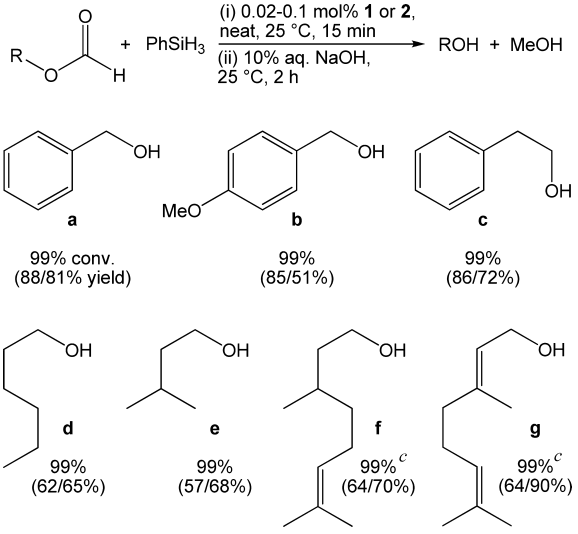

[a]Percent conversion as determined by ^{1}H NMR spectroscopy (TOF = 330 min^{-1} for **a**−**e**; 66 min^{-1} for **f**,**g**). [b]Isolated yields of the corresponding alcohol in parentheses (spectroscopic analysis provided in the Supporting Information). [c]Trial conducted using 0.1 mol % **1** or **2**.

the corresponding alcohols when using 0.1 mol % **1** (**f**,**g**, TOF = 66 min^{-1}), indicating that substrate purity is critically important when maximizing the efficacy of Mn-catalyzed hydrosilylation.

Identification of Catalytically Relevant Species. When analyzing unquenched postcatalysis solutions by multinuclear NMR spectroscopy, partial conversion of **1** to a new Mn complex featuring a ^{1}H NMR triplet at −2.98 ppm (J = 112.4 Hz) and ^{31}P NMR singlet at 69.19 ppm was observed. In an attempt to characterize this compound, one equiv of $PhSiH_3$ was added to a solution of **1** in benzene-d_6. Approximately 20% of the desired product was observed after 24 h at 25 °C; however, longer reaction times did not result in further conversion. Fortunately, treating (^{Ph2PPr}PDI)$MnCl_2$[25] with 2 equiv of $NaEt_3BH$ allowed for the independent preparation and isolation of the C_2-symmetric diamagnetic hydride compound, (^{Ph2PPr}PDI)MnH (eq 1, **2**).Upon formulating **2** as a six-

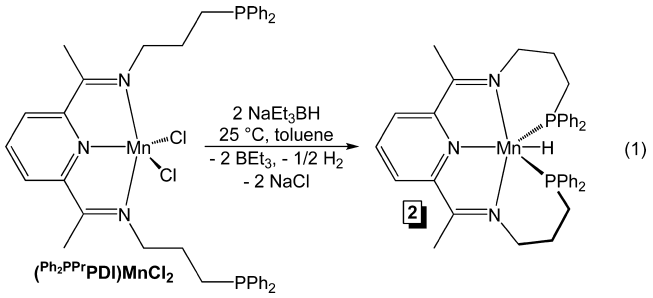

(1)

coordinate monohydride, efforts were made to determine if this compound possesses a traditional octahedral solid-state geometry featuring a low-spin Mn(I) center. Crystallization of **2** from a concentrated toluene solution layered with diethyl ether afforded single crystals suitable for X-ray diffraction analysis, which revealed the geometry about Mn to be a hydride-capped trigonal bipyramid (Figure 3) with N(1)−Mn(1)−N(3) and P(1)−Mn(1)−P(2) angles of 158.81(9)° and 123.85(3)°, respectively (metrical parameters provided in Tables 4 and S2). The Mn(1)−N(1), Mn(1)−N(2), and Mn(1)−N(3) distances were found to be 1.945(2), 1.860(2), and 1.947(2) Å, respectively, suggestive of a low spin Mn center. The imine bond lengths of 1.351(3) and 1.342(3) Å are significantly elongated relative to unreduced PDI chelates (1.28 Å),[27] while the C(2)−C(3) and C(7)−C(8) bonds are contracted to 1.424(4) and 1.418(3) Å, respectively. Comparing these parameters to those of **1** (Table 4)[25] and literature values consistent with PDI reduction,[27] our crystallographic data suggests that **2** possesses a Mn(III) center that is supported by a doubly reduced PDI chelate.

To elucidate the electronic structures of **1** and **2**, density functional theory (DFT) calculations were performed according to methods previously used for our study of [(^{Ph2PPr}PDI)-Mn(CO)][Br].[28] We sampled various possible spin states for **1** and found a doublet state that is energetically preferred in pseudotrigonal bipyramidal coordination geometry. This formally low-spin doublet (S_{Mn} = 1/2) configuration also gave the best agreement with the experimental crystal structure, as enumerated in Table S4. The quartet state, where three Mn-based electrons remain unpaired, is 10.5 kcal/mol higher in energy and is therefore not relevant for the ground state electronic structure of **1**. This finding is in good agreement with our spin state assignment based on experimental observations only.[25] Interestingly, a more detailed analysis of the doublet ground state reveals nonclassical electronic features that were previously not recognized. The calculated Mulliken spin densities of ∼1.5 for Mn and the shapes of the Kohn−Sham orbitals suggest that the electronic structure of complex **1** is best described as a superposition between the two resonance structures shown in Figure 4. The qualitative MO diagram at the left of Figure 4a describes a classical low-spin system that standard ligand field theory may suggest and that we had originally envisioned.[25] There are two doubly occupied MOs that are metal-centered and one that is singly occupied. The PDI ligand electrons reside in one of two nearly degenerate π^*-orbitals (Figure 4b), specifically, the one possessing two nodal planes within the pyridyl moiety labeled as $1\pi^*(1b_1^*)$.

Alternatively, the Mn(II)-d^5 complex may use an open-shell configuration where the Mn-center formally adopts an intermediate-spin configuration exposing three unpaired metal-based electrons that are antiferromagnetically coupled to unpaired electrons in the $1\pi^*$ and $2\pi^*$ PDI-ligand orbitals as illustrated in Figure 4b, explaining the aforementioned α-electron spin density of ∼1.5 on Mn. Based on our calculations, we estimate the J-coupling to be −401 cm^{-1}. This nonclassical electronic structure gives rise to biradical character on the PDI moiety, although the redox state of the ligand has not changed. One plausible way of visualizing how the classical low-spin Mn(II) complex shown in Figure 4a may transform to the nonclassical open-shell configuration is a double electron transfer whereby one α-electron is transferred from the PDI-π^* orbital to the Mn-d_{xy} orbital, while a β-electron from the Mn-d_{xz} orbital is transferred back to the PDI-$2\pi^*$ orbital, as shown in blue and red in Figure 4, respectively (refer to Figure S61).

Formally adding a hydrogen atom oxidatively to **1** affords the Mn(III)-d^4 hydride complex **2**. Five different spin states, namely closed-shell singlet, open-shell singlet, triplet, quintet and septet, were considered. Interestingly, the open-shell singlet state is electronically unstable in the sense that the antiferromagnetically coupled electrons on the PDI ligand

DOI: 10.1021/jacs.7b00879
J. Am. Chem. Soc. 2017, 139, 4901−4915

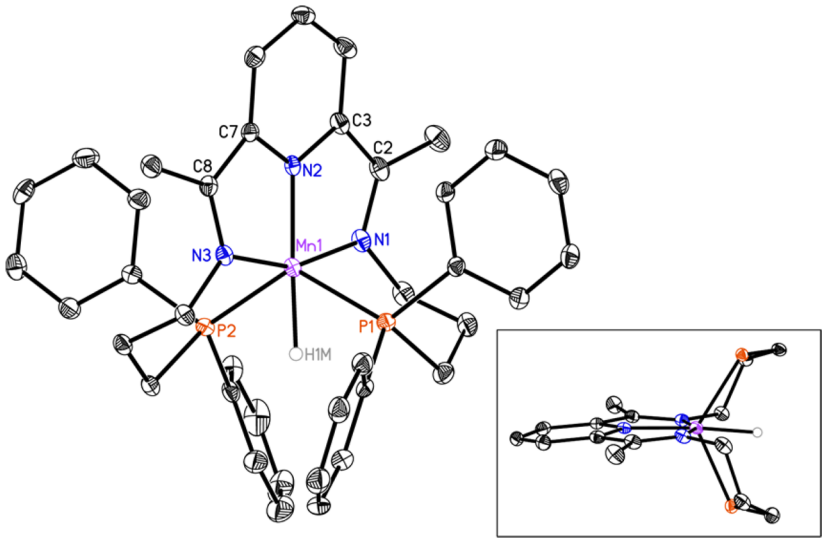

Figure 3. Molecular structure of **2** shown at 30% probability ellipsoids. The asymmetric unit was found to possess a second molecule of **2**, which has been omitted for clarity. Hydrogen atoms other than H1M are also omitted. The inset highlights the capped trigonal bipyramidal geometry about Mn (considering axial imine N atoms) with aryl groups removed for clarity.

Table 4. Bond Lengths (Å) and Angles (deg) Determined for 1 (Previously Reported),[25] 2, and 3

	1	2[a]	3
Mn(1)−N(1)	1.944(2)	1.945(2) [1.951(2)]	2.303(2)
Mn(1)−N(2)	1.887(2)	1.860(2) [1.862(2)]	2.159(2)
Mn(1)−N(3)	1.949(2)	1.947(2) [1.948(2)]	2.270(3)
Mn(1)−P(1)	2.2697(8)	2.2067(8) [2.2117(8)]	2.8055(9)
Mn(1)−P(2)	2.2634(8)	2.2158(7) [2.2064(7)]	
Mn(1)−H(1M)		1.57(3) [1.51(3)]	
Mn(1)−O(1)			2.025(2)
Mn(1)−N(2A)			2.429(2)
N(1)−C(2)	1.354(3)	1.351(3) [1.343(3)]	1.288(4)
N(3)−C(8)	1.355(3)	1.342(3) [1.346(3)]	1.291(4)
C(2)−C(3)	1.416(4)	1.424(4) [1.418(4)]	1.486(4)
C(7)−C(8)	1.414(3)	1.418(3) [1.419(4)]	1.485(4)
N(1)−Mn(1)−N(3)	157.54(9)	158.81(9) [158.64(9)]	139.32(9)
P(1)−Mn(1)−P(2)	105.93(3)	123.85(3) [128.30(3)]	
P(1)−Mn(1)−N(2A)			167.55(6)
N(2)−Mn(1)−H(1M)		175.0(10) [172.9(10)]	
N(2)−Mn(1)−O(1)			174.27(9)

[a]Metrical parameters for second molecule of **2** given in brackets. For additional information, see Figure S1 and Table S2 of the Supporting Information.

and the metal center are unable to remain in different orbitals. The presence of the hydride ligand in the *trans*-position to the PDI-pyridyl moiety impacts the two π^* orbitals in a notably different way: because there is significant N-p orbital component in $1\pi^*$, whereas there is no N-character in $2\pi^*$ Figure 4c, the former is pushed to a much higher energy than the latter. As a consequence, the two excess electrons on the PDI(-II) ligand move into $2\pi^*$ and are paired, as illustrated qualitatively in Figure 5. As a result, the radical character on the PDI ligand that was predicted for **1** is lost; in **2** the two ligand-based electrons are spin-paired.

The hydride ligand has a similarly profound impact on the metal-centered MOs, as highlighted in Figure 5. The $d_{x^2-y^2}$-based MO, which was the lowest energy frontier orbital in **1**, engages in a strong σ-bonding interaction with the hydride ligand, thus pushing the complementary antibonding combination to be the highest energy frontier orbital. Among all spin-states considered, we found that this closed-shell singlet state featuring a diamagnetic PDI dianion[29] is energetically most favorable with the next lowest energy state being the triplet at a relative solution phase free energy of 10.0 kcal/mol. It also gave the best agreement with the experimental structure. The calculated P(1)−Mn(1)−P(2) angle was markedly different between the states; the singlet state calculation gave an angle of 128.2°, which most closely reproduces the experimentally determined values of 123.85 and 128.30°, while the higher spin states provide angles of 148.4° or greater (Table S5). The collection of the metal-centered frontier orbitals can be visualized as that of a classical low-spin system, as illustrated in Figure 5. We suggest that the preference for the low spin state arises from the interaction between the relatively hard Lewis acidic Mn(III) center and the strong field hydride ligand. Moreover, comparing the doublet complex **1** with singlet complex **2** reveals that the latter possesses shorter computed Mn-PDI

DOI: 10.1021/jacs.7b00879
J. Am. Chem. Soc. 2017, 139, 4901−4915

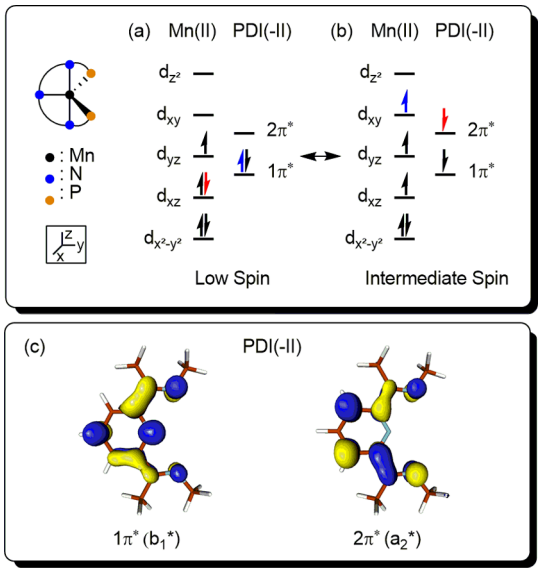

Figure 4. Resonance configurations describing the electronic structure of **1**. (a) Original low spin electronic structure featuring PDI electron pairing. (b) Intermediate spin electronic structure with antiferromagnetic coupling. (c) Frontier MOs of $1\pi^*(b_1^*)$ and $2\pi^*(a_2^*)$.

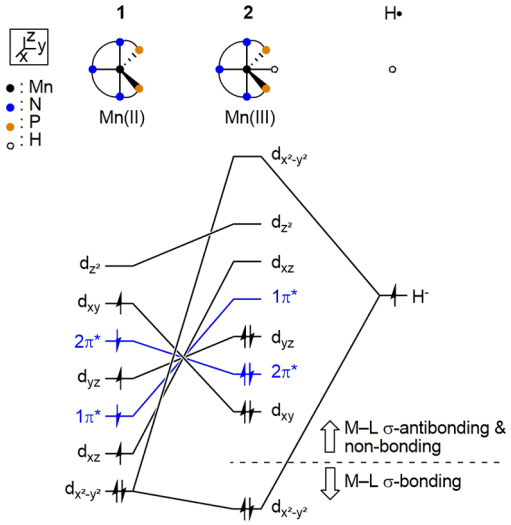

Figure 5. Energy-level diagram for **2**.

bond lengths, with Mn(1)−N(1) and Mn(1)−P(1) distances of 1.950 and 2.202 Å, respectively. Our updated electronic structure descriptions for both compounds are provided in Figure 6; the experimental and computational investigations on **2** reveal a superposition of both available resonance structures as opposed to the localized structure shown.

During our investigation of ketone hydrosilylation,[25] adding 1 mol % **1** to a benzene-d_6 solution containing $PhSiH_3$ and 2,2,2-trifluoroacetophenone resulted in an uncharacteristic bluish-green solution. Complete reduction of this substrate to the quaternary silane product, $PhSi(OCH(CF_3)(Ph))_3$, was observed after 12 h at 25 °C; however, delayed turnover onset was also noted (no conversion after 2 h). Given that all other ketone, aldehyde, ester, and formate solutions remain light brown throughout catalysis, we set out to further investigate the origin of disparate reactivity between 2,2,2-trifluoroacetophenone and the other substrates. When a stoichiometric quantity of 2,2,2-trifluoroacetophenone was added to a THF solution of

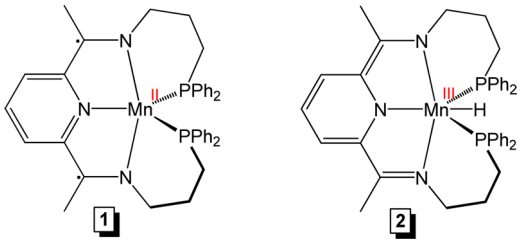

Figure 6. Lewis structures of **1** and **2** that are most consistent with the computed electronic structures.

1, an instantaneous color change from brownish-orange to deep blue was observed. The resulting compound was isolated and found to be ^{1}H NMR silent, although evidence for an uncoordinated phosphine arm was observed by ^{31}P NMR spectroscopy (Figure S47). The solution phase magnetic moment of this product was determined to be 4.4 μ_B (benzene-d_6), which implies an $S_{Mn} = 3/2$ center. Importantly, its electronic spectrum was found to exhibit two absorption maxima at 360 nm (ε = 3410 M^{-1} cm^{-1}) and 612 nm (ε = 3610 M^{-1} cm^{-1}) (Figure S48). Although the extinction coefficients are slightly higher, the wavelengths of these Mn-to-PDI chelate charge transfer bands are nearly identical to those observed for the 5-coordinate monobromide complex, (κ^4-*P,N,N,N*-^{Ph2PPr}PDI)MnBr (361 nm, ε = 3040 M^{-1} cm^{-1}; 614 nm, ε = 2650 M^{-1} cm^{-1}).[28] The magnetic moment and electronic spectrum provide strong evidence that this blue product is (κ^4-*P,N,N,N*-^{Ph2PPr}PDI•)Mn(OC•(Ph)(CF_3)) (eq 2,

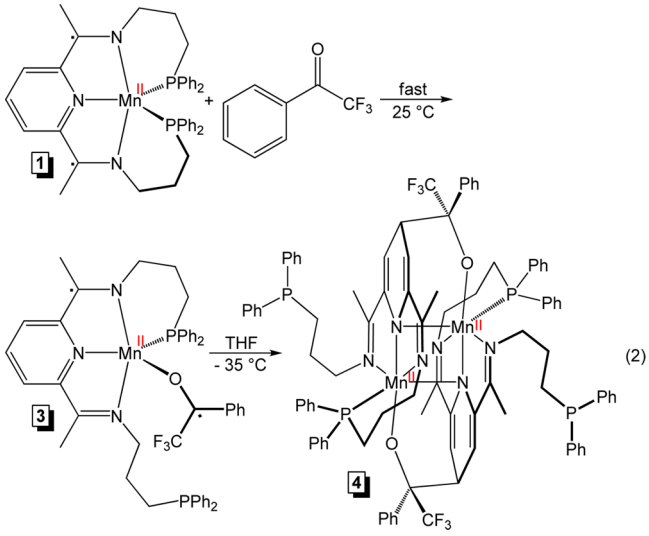

(2)

3), which features a high-spin Mn(II) center that is antiferromagnetically coupled to both PDI and 2,2,2-trifluoroacetophenone radical anions. Observation of radical transfer from one redox-active ligand (PDI) to another (2,2,2-trifluoroacetophenone) is unique and the electron-withdrawing trifluoromethyl substituent renders this substrate more easily reducible than the others that have been screened (which do not react with **1** in the absence of silane).

To further confirm the electronic structure of **3**, attempts were made to obtain single crystals of this compound for X-ray diffraction analysis. Storing a concentrated THF solution of **3** at −35 °C for 24 h afforded light amber crystals that were suitable for X-ray diffraction. The solid-state structure of the light amber complex revealed [(μ-*O*,N_{py}-4-OC(CF_3)(Ph)-4-H-^{Ph2PPr}PDI)-

DOI: 10.1021/jacs.7b00879
J. Am. Chem. Soc. 2017, 139, 4901−4915

Mn]$_2$ (**4**) (Figure 7), which arises from coupling between the PDI radical anion of **3** and the 2,2,2-trifluoroacetophenone

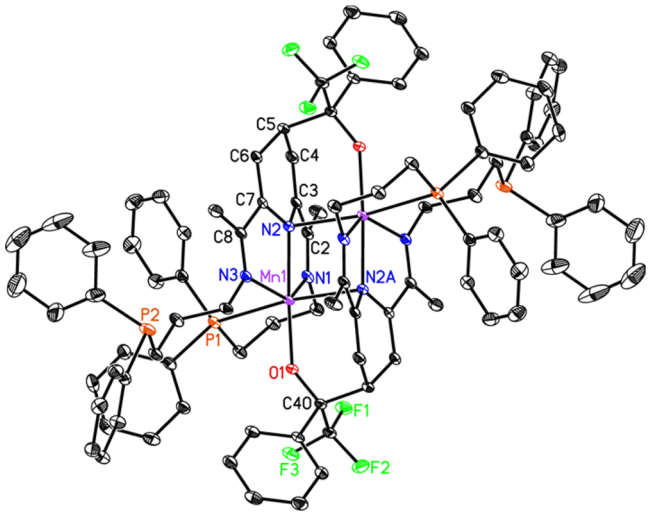

Figure 7. Solid-state structure of **4** shown at 30% probability ellipsoids. Atom labels ending with "A" were generated by symmetry. Hydrogen atoms and three cocrystallized THF molecules per asymmetric unit have been omitted for clarity.

radical anion of a neighboring **3** molecule. Although the PDI radical anion of **3** is delocalized, C−C bond formation takes place at the *para*-position of the central pyridine ring to yield **4**. Complex **4** features a distorted octahedral geometry about Mn(II) consisting of an alkylated κ^4-*P,N,N,N*-^{Ph2PPr}PDI anion, an alkoxide moiety with a short Mn(1)−O(1) contact of 2.025(2) Å, and a weak σ-bonding interaction to the amido functionality of a neighboring chelate [Mn(1)−N(2A) of 2.429(2) Å]. Notably, dimerization of **3** by way of radical coupling destroys the extended π-system of ^{Ph2PPr}PDI. This is clearly seen in the central pyridine ring, where N(2) and C(5) become sp^3-hybridized. The C(3)−C(4) and C(6)−C(7) distances of 1.350(4) and 1.353(4) Å represent true double bonds, while the C(4)−C(5) and C(5)−C(6) contacts of 1.504(5) and 1.503(4) Å indicate a C−C single bond. Likewise, the ^{Ph2PPr}PDI imine substituents in **4** [1.288(4) and 1.291(4) Å] retain double bond character while the C_{imine}−$C_{pyridine}$ distances are representative of single bonds [1.486(4) and 1.485(4) Å]. The Mn(1)-N_{PDI} and Mn(1)−P(1) distances are consistent with a high spin Mn(II) center. Once formed, crystals of **4** are completely insoluble in common solvents.

Kinetic Experiments. Upon isolating compounds relevant to catalysis, the mechanism of **1**-mediated hydrosilylation was investigated. Knowing that **1** possesses an unpaired Mn-based electron (S_{Mn} = 1/2), the possibility that this precatalyst promotes a radical chain mechanism had to be considered. To gain insight, AIBN, a radical chain initiator with $t_{1/2}$ = 1 h at 85 °C, was added to an equimolar mixture of $PhSiH_3$ and diisopropyl ketone under neat conditions. No evidence for carbonyl hydrosilylation was observed after 2 h at 90 °C, suggesting that **1** does not achieve hydrosilylation through a radical initiated pathway. This assessment is further supported by the absence of coupled silane or substrate following catalysis (unused $PhSiH_3$ remains),[25] which are likely termination products of a radical chain mechanism. Adding $PhSiH_3$ and $PhSiD_3$ (50 equiv each) to **1** in the absence of substrate did not result in label scrambling after 12 h at ambient temperature, as judged by ^{1}H NMR spectroscopy.

Considering that **3** is observed upon adding 2,2,2-trifluoroacetophenone to **1**, the possibility that catalysis is achieved following electron transfer to the substrate also had to be evaluated.[30] Radical transfer from a Co/Zr heterobimetallic complex to benzophenone was recently reported by Thomas and co-workers and the resulting ketyl radical is known to undergo concerted homolytic cleavage in the presence of silane to generate silyl ethers.[31] To determine if **1** mediates hydrosilylation in this fashion, kinetic trials were performed to compare the relative rates of carbonyl hydrosilylation using **1**, **2**, and **3**. Because **1**-mediated aldehyde hydrosilylation is exceptionally fast, equimolar solutions of $PhSiH_3$ and diisopropyl ketone in 0.7 mL of benzene-d_6 were added to 1.0 mol % **1**-**3**, and the disappearance of substrate was monitored over time by ^{1}H NMR spectroscopy (Figure 8). As

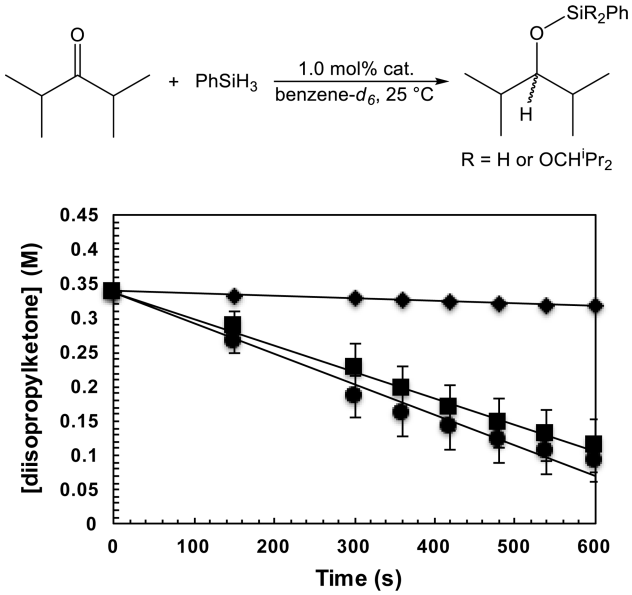

Figure 8. Diisopropyl ketone hydrosilylation at 1.0 mol % catalyst loading in 0.7 mL benzene-d_6. Rates of **1** (●), **2** (■), and **3** (◆) catalyzed reactions are 4.48 × 10^{-4}, 3.87 × 10^{-4}, and 0.36 × 10^{-4} M/s, respectively. Concentrations were determined by ^{1}H NMR integration against anisole internal standard.

anticipated, **1** was found to efficiently convert diisopropyl ketone to a mixture of silyl ethers at a rate of 4.48 × 10^{-4} M/s. Surprisingly, **2** was slightly less active for this transformation (3.87 × 10^{-4} M/s), while radical-transferred complex **3** was considerably less effective (0.36 × 10^{-4} M/s). These rates suggest that **3** must first react with $PhSiH_3$ to enter the catalytic cycle (in benzene-d_6, it takes 48 h for **3** to react with stoichiometric $PhSiH_3$), which is consistent with our prior observation of delayed onset during 2,2,2-trifluoroacetophenone hydrosilylation.[25] Moreover, attempts to achieve diisopropyl ketone hydrosilylation using isolated **4** as the catalyst were unsuccessful, indicating that radical transfer to the substrate is best considered a catalyst deactivation pathway.

With radical chain and radical transfer pathways excluded, **1**-catalyzed diisopropyl ketone hydrosilylation was further examined to establish a rate law. Using 1.0 mol % **1** and a constant concentration of $PhSiH_3$ in benzene-d_6, the rate of disappearance for six different concentrations of diisopropyl

DOI: 10.1021/jacs.7b00879
J. Am. Chem. Soc. 2017, 139, 4901−4915

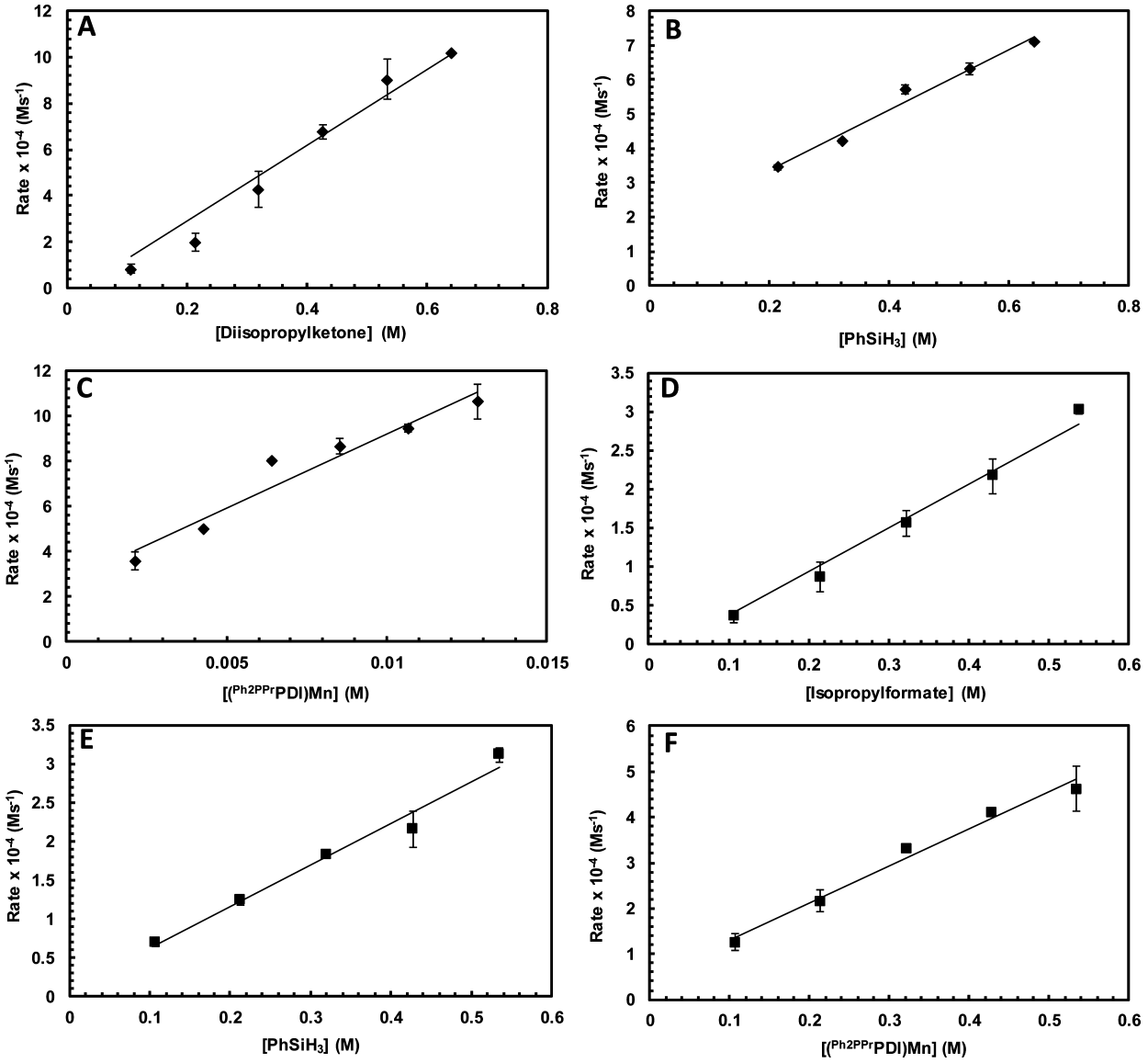

Figure 9. Dependence of [ketone] (A, R^2 = 0.97), [silane] (B, R^2 = 0.98), and [**1**] (C, R^2 = 0.94) on the rate of **1**-catalyzed diisopropyl ketone hydrosilylation. Dependence of formate (D, R^2 = 0.98), silane (E, R^2 = 0.98), and **1** (F, R^2 = 0.96) on the rate of **1**-catalyzed isopropyl formate hydrosilylation.

ketone was determined by ^{1}H NMR spectroscopy with respect to anisole as an internal standard (each data point was collected in triplicate, see Figures S49–S51 for additional information). A first order dependence on diisopropyl ketone concentration was found according to Figure 9A. Likewise, variation of silane and catalyst concentration also revealed a linear dependence on the observed rate (Figure 9B and C). Using the same procedure, the rate law of **1**-catalyzed isopropyl formate dihydrosilylation was determined. When isopropyl formate disappearance was followed under varying concentrations of substrate, $PhSiH_3$, and **1** in benzene-d_6, a first order dependence on each reagent was observed (Figure 9D–F). Therefore, the rate expressions for **1**-catalyzed ketone and formate hydrosilylation can be formulated as

$$\text{rate} = k_{obs}[\mathbf{1}][\text{ketone}][PhSiH_3] \quad (3)$$

$$\text{rate} = k_{obs}[\mathbf{1}][\text{formate}][PhSiH_3] \quad (4)$$

Under identical conditions, a kinetic isotope effect (KIE) for **1**-catalyzed diisopropyl ketone hydrosilylation was established by comparing the rates of substrate disappearance in the presence of stoichiometric $PhSiH_3$ and $PhSiD_3$. Diisopropyl ketone was hydrosilylated using $PhSiH_3$ at a rate of 5.65×10^{-4} M/s, and at a modestly slower rate of 2.53×10^{-4} M/s using $PhSiD_3$, equating to a KIE of 2.2 ± 0.1 (Figure 10A). Primary KIEs of this magnitude are consistent with Si–H bond oxidative addition at (or contributing to) the rate-determining step of the transformation. Since independently prepared **2** mediates carbonyl hydrosilylation at appreciable rates, the same transformations were conducted using this catalyst. A KIE of 4.1 ± 0.6 was observed for **2**-mediated diisopropyl ketone hydrosilylation (Figure 10B), indicating that Si–H bond breaking is the rate-determining step, and that **1** and **2** achieve carbonyl hydrosilylation through different mechanisms.

Upon finding that **1** and **2** operate independently, the carboxylate dihydrosilylation efficiency of each catalyst in the presence of stoichiometric $PhSiH_3$ was assayed by ^{1}H NMR

DOI: 10.1021/jacs.7b00879
J. Am. Chem. Soc. 2017, 139, 4901–4915

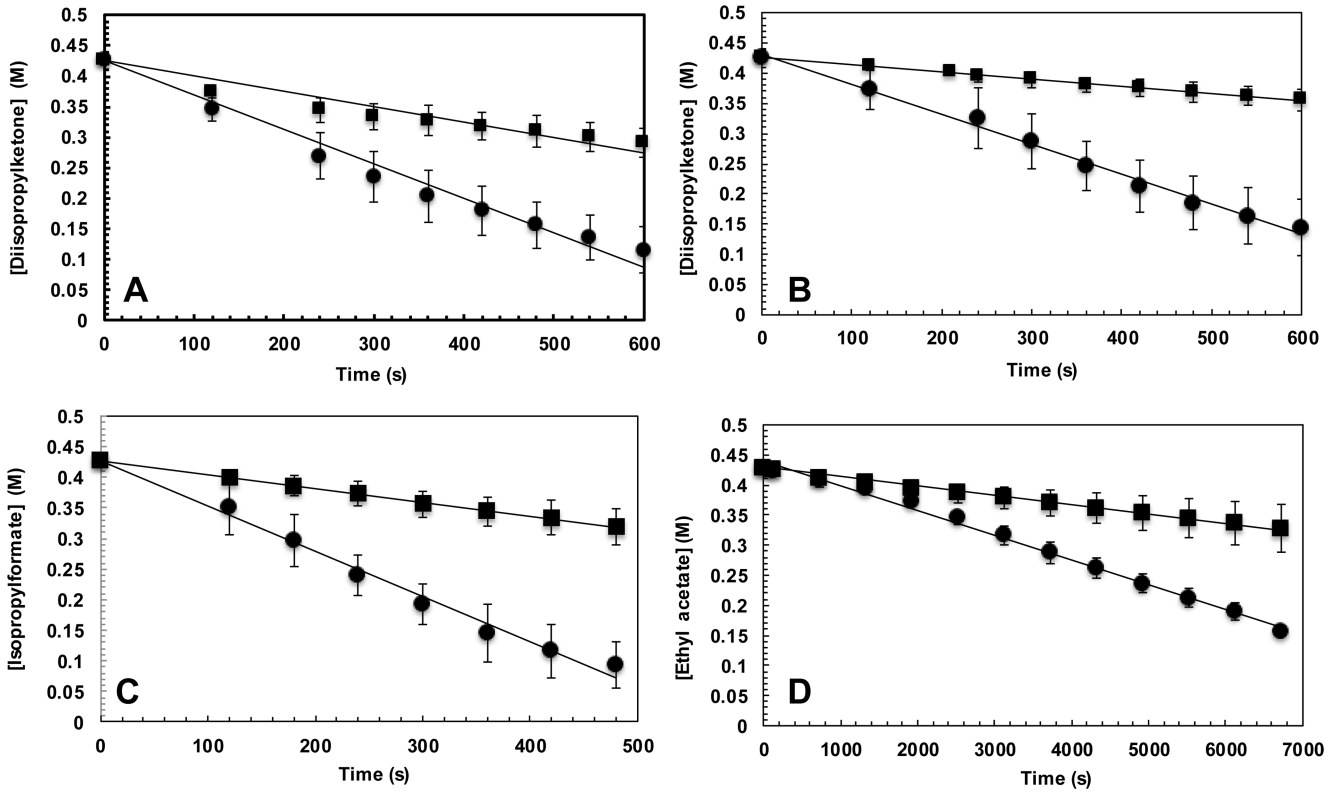

Figure 10. Disappearance of diisopropyl ketone in the presence of $PhSiH_3$ (●) and $PhSiD_3$ (■) catalyzed by 1.0 mol % **1** (A, KIE = 2.2 ± 0.1). Rates are 5.654×10^{-4} M/s ($PhSiH_3$) and 2.534×10^{-4} M/s ($PhSiD_3$). The disappearance of diisopropyl ketone in the presence of $PhSiH_3$ (●) and $PhSiD_3$ (■) catalyzed by 1.0 mol % **2** (**B**, KIE = 4.1 ± 0.6). Rates are 4.96×10^{-4} M/s ($PhSiH_3$) and 1.19×10^{-4} M/s ($PhSiD_3$). Isopropyl formate dihydrosilylation using $PhSiH_3$ and 1.0 mol % of **1** (■, 2.26×10^{-4} M/s) and **2** (●, 7.37×10^{-4} M/s) at 25 °C in benzene-d_6 (C). Ethyl acetate dihydrosilylation using $PhSiH_3$ and 1.0 mol % of **1** (■, 0.16×10^{-4} M/s) and **2** (●, 0.41×10^{-4} M/s) at 25 °C in benzene-d_6 (D).

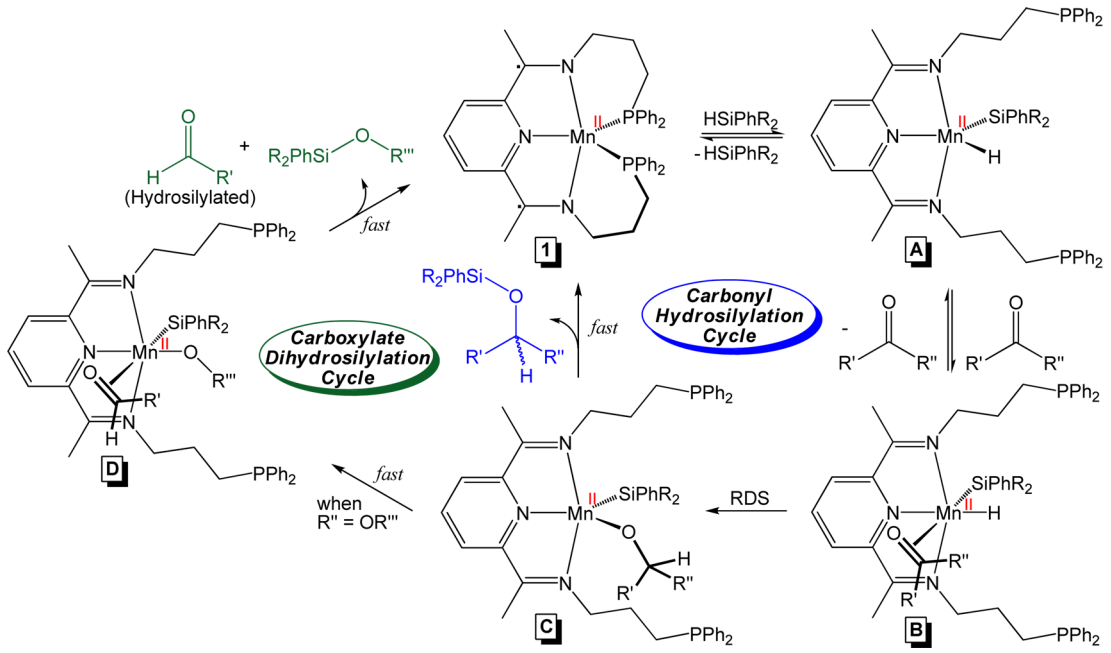

Figure 11. Modified Ojima mechanism for **1**-catalyzed aldehyde (R′ = H, R″ = alkyl or aryl), ketone (R′, R″ = alkyl or aryl), formate (R′ = H, R″ = OR‴; where R‴ = alkyl), and ester (R′ = alkyl, R″ = OR‴; where R‴ = alkyl or aryl) hydrosilylation.

spectroscopy. At 25 °C in benzene-d_6, it was found that 1.0 mol % **1** mediates the reductive cleavage of isopropyl formate at a rate of 2.26×10^{-4} M/s. Surprisingly, **2** was found to be considerably more efficient for this transformation, with an observed rate of 7.37×10^{-4} M/s (Figure 10C). Likewise, **2** was found to catalyze ethyl acetate dihydrosilylation at a faster rate than **1** (Figure 10D), suggesting the mechanism for **2**-mediated carbonyl hydrosilylation is better suited for

DOI: 10.1021/jacs.7b00879
J. Am. Chem. Soc. 2017, 139, 4901−4915

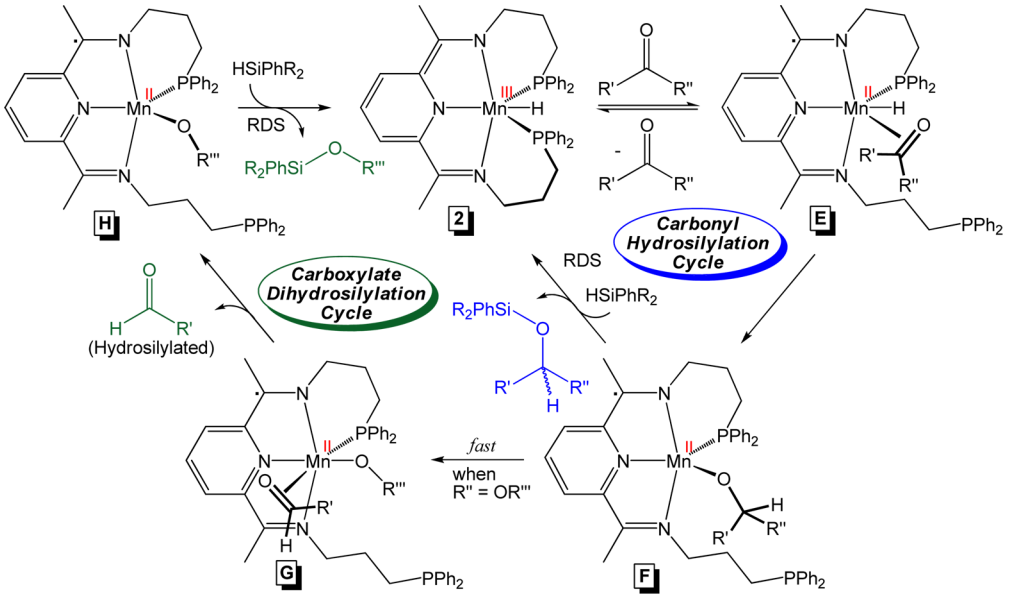

Figure 12. Insertion mechanism for **2**-catalyzed aldehyde (R′ = H, R″ = alkyl or aryl), ketone (R′, R″ = alkyl or aryl), formate (R′ = H, R″ = OR‴; where R‴ = alkyl), and ester (R′ = alkyl, R″ = OR‴; where R‴ = alkyl or aryl) hydrosilylation.

carboxylate reduction than the carbonyl hydrosilylation mechanism for **1**. The synthetic utility of **2** for formate dihydrosilylation has been further demonstrated by repeating each trial in Table 3 using 0.02−0.1 mol % **2**. Each transformation was exothermic and found to reach greater than 99% conversion within 15 min.

Finally, the role of the chelate phosphine donors during catalysis was probed according to different, yet complementary approaches. Since **1** and **2** feature a pentadentate ^{Ph2PPr}PDI chelate, it is logical to hypothesize that phosphine arm dissociation must preclude Si−H activation (in the case of **1**) or substrate binding (at **2**). To determine if exogenous phosphine inhibits the rate of **1**-mediated diisopropyl ketone hydrosilylation, kinetic trials were conducted upon adding 20, 40, and 80 equiv of triphenylphosphine. Phosphine addition had no observable effect on the initial rate of diisopropyl ketone consumption ($6.07 \pm 0.035 \times 10^{-4}$ M/s, Figure S55), suggesting that phosphine coordination does not inhibit catalysis. Moreover, adding 20 equiv of PPh_3 to **1** did not result in observable phosphine displacement by ^{31}P NMR spectroscopy. To determine whether these groups are essential for enabling (PDI)Mn-based carbonyl hydrosilylation, an aryl-substituted PDI precatalyst, ($^{2,6\text{-iPr2Ph}}$PDI)Mn(THF)$_2$,[32] was screened for benzaldehyde hydrosilylation activity. At 1.0 mol % loading in the presence of stoichiometric $PhSiH_3$, complete conversion of the substrate to a mixture of silyl ethers was observed after 10 min, indicating that phosphine donors are not required for (PDI)Mn hydrosilylation activity. Rather, we have found that the phosphine substituents of **1** and **2** serve to stabilize the precatalyst, rendering it less susceptible to decomposition and slightly more tolerant of substrate impurity.

Hydrosilylation Mechanisms. Given the first order dependence of substrate, silane, and **1** on the rate of carbonyl hydrosilylation and carboxylate dihydrosilylation (eqs 3 and 4), a mechanism that incorporates both transformations can be proposed. Considering the spectator role of the ^{Ph2PPr}PDI phosphine donors and the fact that **1** can hydrosilylate sterically demanding ketones such as diisopropyl ketone and dicyclohexyl ketone,[25] this catalyst is believed to operate through an Ojima-like mechanism (Figure 11) that is modified from the general example in Figure 1. The initial step of the transformation involves phosphine dissociation[33] and reversible Si−H oxidative addition to generate the 5-coordinate silyl hydride intermediate **A**. Although formation of **A** is consistent with a primary Si−H(D) KIE of 2.2 ± 0.1, it is not believed to be the rate-determining step. Rather, **A** is believed to reversibly bind substrate to give intermediate **B**, which undergoes insertion into the Mn−H bond to generate **C**. The insertion step is believed to be rate-determining, consistent with having a first-order dependence on both substrate and silane. Moreover, insertion of substrate into the Mn−Si bond (as in Figure 1), is disfavored since it would require formation of a high-energy intermediate that features a bulky tertiary alkyl ligand. In the case of ketone hydrosilylation, **C** undergoes fast reductive elimination to furnish the hydrosilylated product while regenerating catalyst **1**. If Si−H bonds remain, the resulting silyl ether is more reactive than $PhSiH_3$ and further participates in hydrosilylation to form doubly and triply condensed products, explaining the observation of unreacted $PhSiH_3$ after each catalytic reaction.

During **1**-catalyzed formate or ester dihydrosilylation, fast β-alkoxide elimination is believed to occur following insertion to give alkoxide intermediate **D**. Like **C**, **D** reductively eliminates the corresponding silyl ether, but also releases aldehyde upon reforming **1**. Efforts to observe aldehyde produced in situ by ^{1}H NMR spectroscopy have been unsuccessful since aldehydes are quickly reduced in the presence of excess $PhSiH_3$. The carboxylate dihydrosilylation cycle in Figure 11 features β-alkoxide elimination after the rate-determining step, consistent with the rate law established for **1**-catalyzed isopropyl formate dihydrosilylation (eq 4). Throughout the carbonyl hydrosilylation and carboxylate dihydrosilylation cycles in Figure 11, ^{Ph2PPr}PDI acts as a redox noninnocent ligand, allowing the Mn center to remain divalent during catalysis.[34] As indicated, both phosphine donors of ^{Ph2PPr}PDI are free to dissociate and do not inhibit the rate of hydrosilylation.

Knowing $PhSiH_3$ reacts with **1** to generate small quantities of a Mn−H compound under stoichiometric and catalytic

DOI: 10.1021/jacs.7b00879
J. Am. Chem. Soc. 2017, 139, 4901−4915

conditions, and that independently prepared **2** is active for carbonyl hydrosilylation and carboxylate dihydrosilylation, we believe a second pathway contributes to the overall mechanism. It is proposed that intermediate **A** occasionally undergoes silyl ligand loss or transfer to chelate, as observed for isoelectronic Mn dialkyl complexes,[35] to generate **2** or a yet to be identified silylated-PDI variant of **2**, allowing catalysis to proceed through the Mn−H insertion pathway in Figure 12. Starting from **2**, chelate phosphine donor displacement by an incoming carbonyl moiety[33] leads to **E**, which undergoes migratory insertion to yield Mn(II) alkoxide intermediates of type **F**. Since a KIE of 4.1 ± 0.6 was observed for **2**-mediated diisopropyl ketone hydrosilylation, it is believed that the rate-determining step involves σ-bond metathesis between the Mn−O bond of **F** and the Si−H bond of an incoming silane, a pathway that requires more energy than Si−H oxidative addition. This assessment is further supported by kinetic data which shows a dependence on substrate, silane, and **2** during diisopropyl ketone hydrosilylation (Figures S56−S60 of the Supporting Information).

In the case of formate or ester dihydrosilylation, fast β-alkoxide elimination at **F** occurs to form intermediate **G**. Upon losing aldehyde, σ-bond metathesis between the Mn−O bond of **H** and silane can occur to yield the silyl ether product and starting catalyst. As in Figure 11, the aldehyde released in the carboxylate dihydrosilylation cycle in Figure 12 is quickly hydrosilylated under the reaction conditions to yield the corresponding silyl ether. Once phosphine substituent dissociation occurs, the carbonyl and carboxylate hydrosilylation pathways accessed by **2** are believed to proceed at Mn(II); however, the PDI chelate likely remains a radical monoanion throughout catalysis. Considering the mechanistic pathways for **1** and **2**, our kinetic data affirms that the carbonyl hydrosilylation cycle mediated by **1** (Figure 11, right) is faster than the carbonyl hydrosilylation cycle mediated by **2** (Figure 12, right). Conversely, comparing the rates of **1**- and **2**-catalyzed isopropyl formate (Figure 10, **C**) and ethyl acetate reduction (Figure 10, **D**) demonstrates that **2** is the more efficient catalyst for carboxylate dihydrosilylation.

CONCLUSION

By optimizing the conditions of **1**-mediated aldehyde hydrosilylation, TOFs of up to 4900 min^{-1} have been demonstrated and a benzaldehyde hydrosilylation TON of 31 000 has been achieved. Extending this investigation to the reduction of formates revealed dihydrosilylation TOFs of up to 330 min^{-1}, considerably faster than what has been reported for comparable first row metal catalyzed reactions. Importantly, the characterization and study of a Mn−H compound relevant to catalysis, **2**, revealed that this precursor also exhibits exceptional formate dihydrosilylation activity. In contrast, radical transfer from the chelate of **1** to incoming 2,2,2-trifluoroacetophenone has been found to result in catalyst deactivation through intermolecular radical coupling to yield **4**. Kinetic analysis of **1**-mediated carbonyl and formate hydrosilylation revealed a first order dependence on substrate, silane, and catalyst, a primary KIE, and that catalysis is unaffected by exogenous phosphine, indicating that both transformations are achieved through a modified Ojima mechanism. Kinetic analysis of **2**-mediated hydrosilylation revealed a large KIE that has been attributed to rate-determining σ-bond metathesis after substrate insertion. Comparing the activity of **1**- and **2**-mediated hydrosilylation has revealed that **1** is more active for carbonyl hydrosilylation, while **2** is more efficient for carboxylate dihydrosilylation. The mechanistic complexity underlying (PDI)Mn hydrosilylation is surprising and the efforts described herein may prove influential for the study of other leading first row metal catalysts.

EXPERIMENTAL SECTION

General Considerations. Unless otherwise stated, all synthetic manipulations were performed in an MBraun glovebox under an atmosphere of purified nitrogen. Aldrich or Acros anhydrous solvents were purified using a Pure Process Technology solvent system and stored in the glovebox over activated 4 Å molecular sieves and sodium before use. Benzene-d_6 was purchased from Cambridge Isotope Laboratories and dried over 4 Å molecular sieves and potassium before use. $(THF)_2MnCl_2$ and 4-fluorobenzaldehyde were purchased from Acros. 1,3,5,7-Cyclooctatetraene was used as received from Strem Chemicals. Mercury, sodium triethylborohydride, benzaldehyde, *p*-anisaldehyde, *p*-tolualdehyde, *o*-nitrobenzaldehyde, furfural, citral, diisopropyl ketone, 2,2,2-trifluoroacetophenone, *p*-anisyl formate, and citronellyl formate were obtained from Sigma-Aldrich. Phenylsilane, pyridine-3-carboxaldehyde, 4-cyanobenzaldehyde, 4-iodobenzaldehyde, and 4-bromobenzaldehyde were purchased from Oakwood Chemicals. 4-Chlorobenzaldehyde, 2-naphthaldehyde, 3-cyclohexene-1-carboxaldehyde, and anisole were acquired from TCI America. Methyl formate, ethyl formate, benzyl formate, 2-phenylethyl formate, hexyl formate, and isoamyl formate were purchased from TCI America and dried over sieves before use. Geranyl formate was obtained from Santa Cruz Chemicals and dried over sieves before use. 3-(Diphenylphosphino)-1-propylamine,[36] ^{Ph2PPr}PDI,[37] (^{Ph2PPr}PDI)-$MnCl_2$,[25] (^{Ph2PPr}PDI)Mn (**1**),[25] phenylsilane-d_3,[38] and ($^{2,6\text{-}iPr2Ph}$PDI)$Mn(THF)_2$[32] were prepared according to literature procedure.

Solution ^1H nuclear magnetic resonance (NMR) spectra were recorded at room temperature on a Bruker 400, Varian 400, or Varian 500 MHz NMR spectrometer. All ^1H and ^{13}C NMR chemical shifts (ppm) are reported relative to $Si(CH_3)_4$ using ^1H (residual) and ^{13}C chemical shifts of the solvent as secondary standards. ^{31}P NMR data is reported relative to H_3PO_4. Elemental analyses were performed at Robertson Microlit Laboratories Inc. (Ledgewood, NJ) and the Arizona State University CLAS Goldwater Environmental Laboratory (Tempe, AZ). Solution state magnetic susceptibility was determined from Evans method using the Varian 400 MHz NMR spectrometer.

X-ray Crystallography. Single crystals suitable for X-ray diffraction were coated with polyisobutylene oil in the glovebox and transferred to glass fiber with Apiezon N grease, which was then mounted on the goniometer head of a Bruker APEX Diffractometer equipped with Mo Kα radiation (Arizona State University). A hemisphere routine was used for data collection and determination of the lattice constants. The space group was identified and the data was processed using the Bruker SAINT+ program and corrected for absorption using SADABS. The structures were solved using direct methods (SHELXS) completed by subsequent Fourier synthesis and refined by full-matrix, least-squares procedures on [F^2] (SHELXL). The solid-state structure of **2** features two unique molecules in the asymmetric unit. The hydride ligand was located in the difference map for each molecule. The solid-state structure of **4** features three cocrystallized THF molecules per asymmetric unit, one of which was modeled with two partial occupants. The molecular structure of **4** is a dimer that is symmetry generated by an inversion center midway between the two metal atoms. Crystallographic parameters for **2** and **4** can be found in Table S1 of the Supporting Information.

*General Method of Aldehyde Hydrosilylation Using 0.1 mol % **1**.* In the glovebox, a 20 mL scintillation vial was charged with 0.0022 g of **1** (0.0033 mmol). An equimolar mixture of $PhSiH_3$ (3.3 mmol) and aldehyde (3.3 mmol) was then added. ***CAUTION! This reaction is exothermic and vigorous bubbling occurs.*** After 2 min, the solution was exposed to oxygen to deactivate the catalyst, filtered through Celite, and analyzed by ^1H NMR spectroscopy to determine conversion. The silyl ether products were then hydrolyzed by stirring with 2 mL of 10% aqueous NaOH solution for 2 h. The organic layer was extracted with

DOI: 10.1021/jacs.7b00879
J. Am. Chem. Soc. 2017, 139, 4901−4915

diethyl ether (5 × 2 mL) and dried over anhydrous Na_2SO_4, and then the solvent was removed by rotary evaporation (40 °C) to isolate the corresponding alcohol.

*General Method of Aldehyde Hydrosilylation Using 0.01 mol % **1**.* In the glovebox, a 100 mL round-bottom flask was charged with 0.0022 g of **1** (0.0033 mmol). An equimolar mixture of $PhSiH_3$ (33 mmol) and aldehyde (33 mmol) was then added. ***CAUTION! This reaction is exothermic and vigorous bubbling occurs.*** After 2 min, the solution was exposed to oxygen to deactivate the catalyst, filtered through Celite, and analyzed by ^1H NMR spectroscopy to determine conversion. The silyl ether products were then hydrolyzed by stirring with 2 mL of 10% aqueous NaOH solution for 2 h. The organic layer was extracted with diethyl ether (5 × 2 mL), dried over anhydrous Na_2SO_4, and the solvent was removed by rotary evaporation (40 °C) to isolate the corresponding alcohol.

*General Method of Formate Dihydrosilylation Using 0.02 mol % **1** or **2**.* In the glovebox, a 100 mL round-bottom flask was charged with 0.0020 g of catalyst **1** or **2** (0.0033 mmol). An equimolar mixture of $PhSiH_3$ (16 mmol) and aldehyde (16 mmol) was then added. ***CAUTION! This reaction is exothermic and vigorous bubbling occurs.*** After 15 min, the solution was exposed to oxygen to deactivate the catalyst, filtered through Celite, and analyzed by ^1H NMR spectroscopy to determine conversion. The silyl ether products were then hydrolyzed by stirring with 2 mL of 10% aqueous NaOH solution for 2 h. The organic layer was extracted with diethyl ether (5 × 2 mL) and dried over anhydrous Na_2SO_4. The solvent and coproduced methanol were removed by rotary evaporation to isolate the higher molecular weight alcohol.

*General Method of Formate Hydrosilylation Using 0.1 mol % **1** or **2**.* In the glovebox, a 20 mL scintillation vial was charged with 0.0013 g of catalyst **1** or **2** (0.0019 mmol). An equimolar mixture of $PhSiH_3$ (1.9 mmol) and aldehyde (1.9 mmol) was then added. ***CAUTION! This reaction is exothermic and vigorous bubbling occurs.*** After 15 min, the solution was exposed to oxygen to deactivate the catalyst, filtered through Celite, and analyzed by ^1H NMR spectroscopy to determine conversion. The silyl ether products were then hydrolyzed by stirring with 2 mL of 10% aqueous NaOH solution for 2 h. The organic layer was extracted with diethyl ether (5 × 2 mL) and dried over anhydrous Na_2SO_4. The solvent and coproduced methanol were removed by rotary evaporation to isolate the higher molecular weight alcohol.

*Preparation of (^{Ph2PPr}PDI)MnH (**2**).* Under N_2 atmosphere, a 250 mL round-bottom flask was charged with 0.344 g (0.466 mmol) of (^{Ph2PPr}PDI)$MnCl_2$[25] in approximately 80 mL of toluene. The slurry was cooled to liquid N_2 temperature in a cold well for 30 min. A 20 mL scintillation vial was charged with 0.114 g (0.932 mmol) of $NaEt_3BH$ (1 M in toluene) in approximately 10 mL of toluene and also cooled for 30 min. Then the $NaEt_3BH$ solution was added to the slurry of (^{Ph2PPr}PDI)$MnCl_2$ slowly while stirring. The flask was allowed to warm to 25 °C and a deep brownish-green color was observed after 20 min, which continued to darken over time. After 6 h the brownish-green solution was filtered through Celite and the toluene was evacuated to obtain a dark solid. The solid was washed with pentane (4 × 5 mL) and dried again. It was washed quickly with 10 mL of ether (2 × 5 mL) to remove any free ligand generated in the reaction. It was then filtered through Celite using 15 mL of toluene. The toluene was removed in vacuo, and the residue was dissolved in a minimum amount of diethyl ether and placed at −35 °C overnight. Dark green crystals identified as **2** (0.125 g, 0.187 mmol, 40%) were collected after drying. Analysis for $C_{39}H_{42}N_3P_2Mn$: Calcd C, 69.94%; H, 6.32%; N, 6.27%. Found: C, 68.26%; H, 6.44%; N, 5.88%. ^1H NMR (benzene-d_6): δ (ppm) = 8.17 (d, J_{H-H} = 8.1 Hz, 2H, *pyridine*), 7.76 (t, J_{H-H} = 8.1 Hz, 1H, *pyridine*), 7.47 (t, J_{H-H} = 8.1 Hz, 4H, *phenyl*), 7.09 (m, 4H, *phenyl*), 6.61 (m, 6H, *phenyl*), 5.66 (t, J_{H-H} = 8.1 Hz, 4H, *phenyl*), 4.50 (d, J_{H-H} = 11.4 Hz, 2H, $-CH_2$), 2.83 (t, J_{H-H} = 11.2 Hz, 2H, $-CH_2$), 2.48 (broad m, 4H, $-CH_2$), 2.34 (s, 6H, CH_3), 1.78 (broad m, 2H, $-CH_2$), 1.36 (broad m, 2H, $-CH_2$), 1.26 (broad m, 2H, $-CH_2$), −2.98 (t, J_{P-H} = 112.4 Hz, 1H, Mn-*H*). ^{13}C NMR (benzene-d_6): δ (ppm) = 154.57 (C═N), 151.46 (*Ar*), 144.10 (dd, *J* = 22.3, 18.6 Hz, *Ar*), 137.64 (*Ar*), 133.48 (dd, *J* = 18.3, 13.9 Hz, *Ar*), 133.01 (t, *J* = 6.4 Hz, *Ar*), 131.35 (t, *J* = 3.7 Hz, *Ar*), 129.42 (*Ar*), 129.21 (t, *J* = 5.1 Hz, *Ar*), 128.98 (*Ar*), 115.29 (*Ar*), 110.37 (*Ar*), 57.47 (CH_2), 33.18 (d, *J* = 19.2, 16.9 Hz, PCH_2), 29.70 (CH_2), 14.40 (CH_3). $^{31}P\{^1H\}$ NMR (benzene-d_6): δ (ppm) = 69.19 (s).

*Preparation of (^{Ph2PPr}PDI·)Mn(OC·(Ph)(CF_3)) (**3**).* Under an inert atmosphere, a 20 mL scintillation vial was charged with 0.108 g (0.162 mmol) of **1** in approximately 10 mL benzene. To the dark brown solution, 0.023 mL (0.162 mmol) of 2,2,2-trifluoroacetophenone was added. The solution turned deep blue in color immediately. It was stirred for 1 h and then filtered through Celite. The filtrate was dried under vacuum to isolate a blue residue. After repeated washing with diethyl ether (5 × 3 mL) followed by drying *in vacuo*, 0.078 g (0.092 mmol, 56%) of a dark blue solid identified as **3** was isolated. Analysis for $C_{47}H_{46}N_3P_2MnOF_3$: Calcd C, 66.77%; H, 5.48%; N, 4.96%. Found: C, 66.69%; H, 5.35%; N, 4.78%. ^1H NMR (benzene-d_6): δ (ppm) No resonances observed. Magnetic moment (Evans method, benzene-d_6): μ_{eff} = 4.4 μ_B. UV−vis (from 7 independent concentrations in toluene, Figure S48): λ_{max} = 360 nm (ε = 3410 M^{-1} cm^{-1}), 612 nm (ε = 3610 M^{-1} cm^{-1}).

*Preparation of [(μ-O,N_{py}-4-OC(CF_3)(Ph)-4-H-^{Ph2PPr}PDI)Mn]$_2$ (**4**).* A concentrated THF solution of **3** (0.078 g, 0.092 mmol) was placed at −35 °C for 24 h. The blue solution was removed and the remaining solid was washed with toluene (3 × 2 mL) and Et_2O (2 × 2 mL). Drying in vacuo yielded 0.027 g (0.016 mmol, 17%) of amber crystals identified as **4**. Analysis for $C_{94}H_{92}N_6P_4Mn_2O_2F_6$: Calcd C, 66.77%; H, 5.48%; N, 4.96%. Found: C, 66.02%; H, 5.66%; N, 4.75%. ^1H NMR (benzene-d_6): δ (ppm) No resonances observed.

General Method for Kinetic Data Collection. In the glovebox, a J. Young tube was charged with a benzene-d_6 (0.7 mL) solution of 0.002 g of catalyst. The tube was placed into a liquid N_2 jacketed cold well to freeze the catalyst solution. While frozen, $PhSiH_3$ was added, followed by the substrate (ketone or ester). Finally, 10 μL of anisole was added as an internal standard. The tube was sealed under N_2 atmosphere and promptly transferred into a dewar filled with liquid N_2. After warming the reaction mixture to room temperature, a ^1H NMR experiment was quickly started and spectral data was collected at 1 min (or 30 s) intervals. The substrate consumption rate was calculated by integrating the starting material and product with respect to anisole. Each experiment was duplicated or triplicated to determine an average rate and standard deviation.

Computational Data. All calculations were performed using density functional theory[39] (DFT) implemented in the Jaguar 9.1[40] suite of ab initio quantum chemistry programs. The geometry optimization calculations were carried out with the PBE[41] functional. The 6-31G** basis set[42] was used for all atoms. The energies of the optimized structures were reevaluated by single-point calculations using PBE-D3[43] functional along with Dunning's correlation consistent triple-ζ basis set cc-pVTZ(-f)[44] that includes a double set of polarization functions.

The optimized stationary points were confirmed through analytic computation of harmonic force constants. The analytical vibrational frequencies computed with the PBE/6-31G** level of theory were used to derive zero point energy and vibrational entropy corrections from the unscaled frequencies which have only one imaginary frequency. Solvation energies were evaluated by a self-consistent reaction field (SCRF) approach[45] using a dielectric constant of ε = 2.284 along with the optimized gas phase structures.

The energy components were computed with the protocol below (eqs 5−8), with *G*(gas) being the Gibbs free energy in gas phase; *G*(solv) being the free energy of solvation; *H*(gas) being the enthalpy in gas phase; *T* being the temperature; *S*(gas) the entropy in gas phase; *E*(SCF) being the self-consistent field energy; ZPE being the zero point energy. The spin−spin coupling constant *J* for the antiferromagnetic coupling in complex **1** has been evaluated using Noodleman's spin-projection technique (eq 9).[46]

$$\Delta G(\text{sol}) = \Delta G(\text{gas}) + \Delta G(\text{solv}) \quad (5)$$

$$\Delta G(\text{gas}) = \Delta H(\text{gas}) - T\Delta S(\text{gas}) \quad (6)$$

DOI: 10.1021/jacs.7b00879
J. Am. Chem. Soc. 2017, 139, 4901−4915

$$\Delta H(\text{gas}) = \Delta E(\text{SCF}) + \Delta\text{ZPE} + \Delta C^{v}T + \Delta(PV) \quad (7)$$

$$\Delta H(\text{gas}) \approx \Delta E(\text{SCF}) + \Delta\text{ZPE} \quad (8)$$

$$J = \frac{E_{BS} - E_{HS}}{2S_{HS}S_{BS} + S_{BS}} \quad (9)$$

■ ASSOCIATED CONTENT

Supporting Information

The Supporting Information is available free of charge on the ACS Publications website at DOI: 10.1021/jacs.7b00879.

Detailed hydrosilylation procedures, crystallographic information for **2** (CCDC 1518909) and **4** (CCDC 1518910), NMR spectroscopic data, Cartesian coordinates of the DFT-optimized structures, and computational details (PDF)

Crystal data for (^{Ph2PPr}PDI)MnH and [(μ-O,N_{py}-4-OC(CF_3)(Ph)-4-H-^{Ph2PPr}PDI)Mn]$_2$ (CIF)

■ AUTHOR INFORMATION

Corresponding Authors

*mbaik2805@kaist.ac.kr

*ryan.trovitch@asu.edu

ORCID

Mu-Hyun Baik: 0000-0002-8832-8187

Ryan J. Trovitch: 0000-0003-4935-6780

Notes

The authors declare the following competing financial interest(s): T. K. M. and R. J. T. retain rights to 1 and 2 through US20160176908 and WO2014201082. Catalyst **1** has been commercialized through Sigma-Aldrich Corporation (a subsidiary of Merck KGaA).

■ ACKNOWLEDGMENTS

Acknowledgment is made to the Donors of the American Chemical Society Petroleum Research Fund for support of this research. M.-H. B. and R. J. T. would like to thank the Research Corporation for Science Advancement for fostering collaboration through Scialog. We thank the Institute for Basic Science (IBS-R10-D1) in Korea for financial support.

■ REFERENCES

(1) For early hydrosilylation reviews, see: (a) Speier, J. L. *Adv. Organomet. Chem.* **1979**, *17*, 407−447. (b) Ojima, I. *Chem. Org. Silicon Compd.* **1989**, *2*, 1479−1526.

(2) Speier, J. L.; Webster, J. A.; Barnes, G. H. *J. Am. Chem. Soc.* **1957**, *79*, 974−979.

(3) Troegel, D.; Stohrer, J. *Coord. Chem. Rev.* **2011**, *255*, 1440−1459.

(4) Chalk, A. J.; Harrod, J. F. *J. Am. Chem. Soc.* **1965**, *87*, 16−21.

(5) Maruyama, Y.; Yamamura, K.; Nakayama, I.; Yoshiuchi, K.; Ozawa, F. *J. Am. Chem. Soc.* **1998**, *120*, 1421−1429 and references therein.

(6) For leading examples, see: (a) Deutsch, C.; Krause, N.; Lipshutz, B. H. *Chem. Rev.* **2008**, *108*, 2916−2927. (b) Morris, R. H. *Chem. Soc. Rev.* **2009**, *38*, 2282−2291. (c) Riener, K.; Högerl, M. P.; Gigler, P.; Kühn, F. E. *ACS Catal.* **2012**, *2*, 613−621. (d) Bleith, T.; Wadepohl, H.; Gade, L. H. *J. Am. Chem. Soc.* **2015**, *137*, 2456−2459.

(7) Osborn, J. A.; Jardine, F. H.; Young, J. F.; Wilkinson, G. *J. Chem. Soc. A* **1966**, 1711−1732.

(8) (a) Ojima, I.; Nihonyanagi, M.; Kogure, T.; Kumagai, M.; Horiuchi, S.; Nakatsugawa, K.; Nagai, Y. *J. Organomet. Chem.* **1975**, *94*, 449−461. (b) Reyes, C.; Prock, A.; Giering, W. P. *Organometallics* **2002**, *21*, 546−554.

(9) (a) Schneider, N.; Finger, M.; Haferkemper, C.; Bellemin-Laponnaz, S.; Hofmann, P.; Gade, L. H. *Angew. Chem., Int. Ed.* **2009**, *48*, 1609−1613. (b) Schneider, N.; Finger, M.; Haferkemper, C.; Bellemin-Laponnaz, S.; Hofmann, P.; Gade, L. H. *Chem. - Eur. J.* **2009**, *15*, 11515−11529.

(10) (a) Gutsulyak, D. V.; Vyboishchikov, S. F.; Nikonov, G. I. *J. Am. Chem. Soc.* **2010**, *132*, 5950−5951. (b) Park, S.; Brookhart, M. *Organometallics* **2010**, *29*, 6057−6064. (c) Lipke, M. C.; Tilley, T. D. *J. Am. Chem. Soc.* **2014**, *136*, 16387−16398.

(11) For first-row metal alkene hydrosilylation catalysts, see: (a) Tondreau, A. M.; Atienza, C. C. H.; Weller, K. J.; Nye, S. A.; Lewis, K. M.; Delis, J. G. P.; Chirik, P. J. *Science* **2012**, *335*, 567−570. (b) Hojilla Atienza, C. C.; Tondreau, A. M.; Weller, K. J.; Lewis, K. M.; Cruse, R. W.; Nye, S. A.; Boyer, J. L.; Delis, J. G. P.; Chirik, P. J. *ACS Catal.* **2012**, *2*, 2169−2172. (c) Tondreau, A. M.; Atienza, C. C. H.; Darmon, J. M.; Milsmann, C.; Hoyt, H. M.; Weller, K. J.; Nye, S. A.; Lewis, K. M.; Boyer, J.; Delis, J. G. P.; Lobkovsky, E.; Chirik, P. J. *Organometallics* **2012**, *31*, 4886−4893. (d) Peng, D.; Zhang, Y.; Du, X.; Zhang, L.; Leng, X.; Walter, M. D.; Huang, Z. *J. Am. Chem. Soc.* **2013**, *135*, 19154−19166. (e) Srinivas, V.; Nakajima, Y.; Ando, W.; Sato, K.; Shimada, S. *Catal. Sci. Technol.* **2015**, *5*, 2081−2084. (f) Chen, J.; Cheng, B.; Cao, M.; Lu, Z. *Angew. Chem., Int. Ed.* **2015**, *54*, 4661−4664. (g) Steiman, T. J.; Uyeda, C. *J. Am. Chem. Soc.* **2015**, *137*, 6104−6110. (h) Sunada, Y.; Noda, D.; Soejima, H.; Tsutsumi, H.; Nagashima, H. *Organometallics* **2015**, *34*, 2896−2906. (i) Buslov, I.; Becouse, J.; Mazza, S.; Montandon-Clerc, M.; Hu, X. *Angew. Chem., Int. Ed.* **2015**, *54*, 14523−14526. (j) Chen, C.; Hecht, M. B.; Kavara, A.; Brennessel, W. W.; Mercado, B. Q.; Weix, D. J.; Holland, P. L. *J. Am. Chem. Soc.* **2015**, *137*, 13244−13247. (k) Noda, D.; Tahara, A.; Sunada, Y.; Nagashima, H. *J. Am. Chem. Soc.* **2016**, *138*, 2480−2483.

(12) For leading Fe carbonyl hydrosilylation catalysts, see: (a) Tondreau, A. M.; Lobkovsky, E.; Chirik, P. J. *Org. Lett.* **2008**, *10*, 2789−2792. (b) Tondreau, A. M.; Darmon, J. M.; Wile, B. M.; Floyd, S. K.; Lobkovsky, E.; Chirik, P. J. *Organometallics* **2009**, *28*, 3928−3940. (c) Kandepi, V. V. K. M.; Cardoso, J. M. S.; Peris, E.; Royo, B. *Organometallics* **2010**, *29*, 2777−2782. (d) Yang, J.; Tilley, T. D. *Angew. Chem., Int. Ed.* **2010**, *49*, 10186−10188. (e) Bhattacharya, P.; Krause, J. A.; Guan, H. *Organometallics* **2011**, *30*, 4720−4729. (f) Ruddy, A. J.; Kelly, C. M.; Crawford, S. M.; Wheaton, C. A.; Sydora, O. L.; Small, B. L.; Stradiotto, M.; Turculet, L. *Organometallics* **2013**, *32*, 5581−5588. (g) Blom, B.; Enthaler, S.; Inoue, S.; Irran, E.; Driess, M. *J. Am. Chem. Soc.* **2013**, *135*, 6703−6713.

(13) For leading Co carbonyl hydrosilylation catalysts, see: (a) Brunner, H.; Amberger, K. *J. Organomet. Chem.* **1991**, *417*, C63−C65. (b) Yu, F.; Zhang, X.-C.; Wu, F.-F.; Zhou, J.-N.; Fang, W.; Wu, J.; Chan, A. S. C. *Org. Biomol. Chem.* **2011**, *9*, 5652. (c) Sauer, D. C.; Wadepohl, H.; Gade, L. H. *Inorg. Chem.* **2012**, *51*, 12948−12958. (d) Niu, Q.; Sun, H.; Li, X.; Klein, H.-F.; Flörke, U. *Organometallics* **2013**, *32*, 5235−5238. (e) Zhou, H.; Sun, H.; Zhang, S.; Li, X. *Organometallics* **2015**, *34*, 1479−1486. (f) Nesbit, M. A.; Suess, D. L. M.; Peters, J. C. *Organometallics* **2015**, *34*, 4741−4752.

(14) For leading Ni carbonyl hydrosilylation catalysts, see: (a) Chakraborty, S.; Krause, J. A.; Guan, H. *Organometallics* **2009**, *28*, 582−586. and references therein. (b) Tran, B. L.; Pink, M.; Mindiola, D. J. *Organometallics* **2009**, *28*, 2234−2243. (c) Postigo, L.; Royo, B. *Adv. Synth. Catal.* **2012**, *354*, 2613−2618. (d) Bheeter, L. P.; Henrion, M.; Brelot, L.; Darcel, C.; Chetcuti, M. J.; Sortais, J.-B.; Ritleng, V. *Adv. Synth. Catal.* **2012**, *354*, 2619−2624. (e) Porter, T. M.; Hall, G. B.; Groy, T. L.; Trovitch, R. J. *Dalton Trans.* **2013**, *42*, 14689−14692. (f) MacMillan, S. N.; Harman, W. H.; Peters, J. C. *Chem. Sci.* **2014**, *5*, 590−597.

(15) For leading Cu carbonyl hydrosilylation catalysts, see: (a) Brunner, H.; Miehling, W. *J. Organomet. Chem.* **1984**, *275*, C17−C21. (b) Sirol, S.; Courmarcel, J.; Mostefai, N.; Riant, O. *Org. Lett.* **2001**, *3*, 4111−4113. (c) Lipshutz, B. H.; Noson, K.; Chrisman, W. *J. Am. Chem. Soc.* **2001**, *123*, 12917−12918. (d) Lipshutz, B. H.; Noson, K.; Chrisman, W.; Lower, A. *J. Am. Chem. Soc.* **2003**, *125*, 8779−8789. (e) Kaur, H.; Zinn, F. K.; Stevens, E. D.; Nolan, S. P. *Organometallics* **2004**, *23*, 1157−1160. (f) Lee, D.; Yun, J. *Tetrahedron*

DOI: 10.1021/jacs.7b00879
J. Am. Chem. Soc. 2017, 139, 4901−4915

Lett. **2004**, *45*, 5415−5417. (g) Wu, J.; Ji, J.-X.; Chan, A. S. C. *Proc. Natl. Acad. Sci. U. S. A.* **2005**, *102*, 3570−3575. (h) Díez-González, S.; Kaur, H.; Zinn, F. K.; Stevens, E. D.; Nolan, S. P. *J. Org. Chem.* **2005**, *70*, 4784−4796. (i) Díez-González, S.; Scott, N. M.; Nolan, S. P. *Organometallics* **2006**, *25*, 2355−2358. (j) Lipshutz, B. H.; Lower, A.; Kucejko, R. J.; Noson, K. *Org. Lett.* **2006**, *8*, 2969−2972. (k) Mostefaï, N.; Sirol, S.; Courmarcel, J.; Riant, O. *Synthesis* **2007**, *2007*, 1265−1271. (l) Fujihara, T.; Semba, K.; Terao, J.; Tsuji, Y. *Angew. Chem., Int. Ed.* **2010**, *49*, 1472−1476. (m) Díez-González, S.; Escudero-Adán, E.; Benet-Buchholz, J.; Stevens, E. D.; Slawin, A. M. Z.; Nolan, S. P. *Dalton Trans.* **2010**, *39*, 7595−7606. (n) Zhang, X.-C.; Wu, F.-F.; Li, S.; Zhou, J.-N.; Wu, J.; Li, N.; Fang, W.; Lam, K. H.; Chan, A. S. C. *Adv. Synth. Catal.* **2011**, *353*, 1457−1462. (o) Yu, F.; Zhou, J.-N.; Zhang, X.-C.; Sui, Y.-Z.; Wu, F.-F.; Xie, L.-J.; Chan, A. S. C.; Wu, J. *Chem. - Eur. J.* **2011**, *17*, 14234−14240. (p) Albright, A.; Gawley, R. E. *J. Am. Chem. Soc.* **2011**, *133*, 19680−19683. (q) Roy, S. R.; Sau, S. C.; Mandal, S. K. *J. Org. Chem.* **2014**, *79*, 9150−9160.

(16) For leading Zn carbonyl hydrosilylation catalysts, see: (a) Mimoun, H. *J. Org. Chem.* **1999**, *64*, 2582−2589. (b) Mastranzo, V. M.; Quintero, L.; Anaya de Parrodi, C.; Juaristi, E.; Walsh, P. J. *Tetrahedron* **2004**, *60*, 1781−1789. (c) Bette, V.; Mortreux, A.; Savoia, D.; Carpentier, J.-F. *Tetrahedron* **2004**, *60*, 2837−2842. (d) Bette, V.; Mortreux, A.; Savoia, D.; Carpentier, J.-F. *Adv. Synth. Catal.* **2005**, *347*, 289−302. (e) Gérard, S.; Pressel, Y.; Riant, O. *Tetrahedron: Asymmetry* **2005**, *16*, 1889−1891. (f) Gajewy, J.; Kwit, M.; Gawroński, J. *Adv. Synth. Catal.* **2009**, *351*, 1055−1063. (g) Enthaler, S.; Schröder, K.; Inoue, S.; Eckhardt, B.; Junge, K.; Beller, M.; Drie*β*, M. *Eur. J. Org. Chem.* **2010**, *2010*, 4893−4901. (h) Pang, S.; Peng, J.; Li, J.; Bai, Y.; Xiao, W.; Lai, G. *Chirality* **2013**, *25*, 275−280. (i) Boone, C.; Korobkov, I.; Nikonov, G. I. *ACS Catal.* **2013**, *3*, 2336−2340. (j) Łowicki, D.; Bezłada, A.; Mlynarski, J. *Adv. Synth. Catal.* **2014**, *356*, 591−595. (k) Lummis, P. A.; Momeni, M. R.; Lui, M. W.; McDonald, R.; Ferguson, M. J.; Miskolzie, M.; Brown, A.; Rivard, E. *Angew. Chem., Int. Ed.* **2014**, *53*, 9347−9351. (l) Rit, A.; Zanardi, A.; Spaniol, T. P.; Maron, L.; Okuda, J. *Angew. Chem., Int. Ed.* **2014**, *53*, 13273−13277. (m) Sattler, W.; Ruccolo, S.; Chaijan, M. R.; Allah, T. N.; Parkin, G. *Organometallics* **2015**, *34*, 4717−4731.

(17) (a) Enthaler, S.; Junge, K.; Beller, M. *Angew. Chem., Int. Ed.* **2008**, *47*, 3317−3321. (b) Plietker, B. *Iron Catalysis in Organic Chemistry: Reactions and Applications*; Wiley-VCH: Weinheim, Germany, 2008.

(18) Collman, J. P.; Hegedus, L. S.; Norton, J. R.; Finke, R. G. In *Principles and Applications of Organotransition Metal Chemistry*; University Science Books: Sausalito, CA, 1987; pp 306−333.

(19) For example, in Metsänen, T. T.; Gallego, D.; Szilvási, T.; Driess, M.; Oestreich, M. *Chem. Sci.* **2015**, *6*, 7143−7149. A peripheral mechanism which does not involve iron mediated organometallic pathways has been proposed. While the Ni and Zn catalysts described in refs 14a and 16m are believed to catalyze carbonyl hydrosilylation via insertion into M−H followed by Si−H *σ*-bond metathesis, the leading Co catalyst for this transformation (ref 13f) relies on borane-assisted Si−H activation and carbonyl insertion into the resulting Co−Si bond.

(20) (a) Valyaev, D. A.; Lavigne, G.; Lugan, N. *Coord. Chem. Rev.* **2016**, *308*, 191−235. (b) Trovitch, R. J. *Synlett* **2014**, *25*, 1638−1642.

(21) (a) Igarashi, M.; Fuchikami, T. *Tetrahedron Lett.* **2001**, *42*, 1945−1947. (b) Zheng, J.; Chevance, S.; Darcel, C.; Sortais, J.-B. *Chem. Commun.* **2013**, *49*, 10010−10012.

(22) (a) Mao, Z.; Gregg, B. T.; Cutler, A. R. *J. Am. Chem. Soc.* **1995**, *117*, 10139−10140. (b) DiBiase Cavanaugh, M.; Gregg, B. T.; Cutler, A. R. *Organometallics* **1996**, *15*, 2764−2769. (c) Son, S. U.; Paik, S.-J.; Lee, I. S.; Lee, Y.-A.; Chung, Y. K.; Seok, W. K.; Lee, H. N. *Organometallics* **1999**, *18*, 4114−4118. (d) Son, S. U.; Paik, S.-J.; Chung, Y. K. *J. Mol. Catal. A: Chem.* **2000**, *151*, 87−90. (e) Zheng, J.; Elangovan, S.; Valyaev, D. A.; Brousses, R.; César, V.; Sortais, J.-B.; Darcel, C.; Lugan, N.; Lavigne, G. *Adv. Synth. Catal.* **2014**, *356*, 1093−1097. (f) During preparation of the manuscript, it was proposed that (Cp)Mn(I) catalysts achieve carbonyl hydrosilylation through a modified Ojima mechanism. For leading work in this area, please see: Valyaev, D. A.; Wei, D.; Elangovan, S.; Cavailles, M.; Dorcet, V.; Sortais, J.-B.; Darcel, C.; Lugan, N. *Organometallics* **2016**, *35*, 4090−4098.

(23) Ghosh, C.; Mukhopadhyay, T. K.; Flores, M.; Groy, T. L.; Trovitch, R. J. *Inorg. Chem.* **2015**, *54*, 10398−10406.

(24) Chidara, V. K.; Du, G. *Organometallics* **2013**, *32*, 5034−5037.

(25) Mukhopadhyay, T. K.; Flores, M.; Groy, T. L.; Trovitch, R. J. *J. Am. Chem. Soc.* **2014**, *136*, 882−885.

(26) Many transition metal catalysts have been described for the dihydrosilylation of carboxylates. The leading turnover frequency for each metal previously reported to mediate selective acyl C−O cleavage is provided: (a) For Ti (TOF = 33 h^{-1}): Barr, K. J.; Berk, S. C.; Buchwald, S. L. *J. Org. Chem.* **1994**, *59*, 4323−4326. (b) For V (TOF = 0.8 h^{-1}): Pehlivan, L.; Métay, E.; Laval, S.; Dayoub, W.; Delbrayelle, D.; Mignani, G.; Lemaire, M. *Eur. J. Org. Chem.* **2011**, *2011*, 7400−7406. (c) For Mn (TOF = 18 h^{-1}): see ref 25. (d) For Fe (TOF as high as 100 h^{-1}): see ref 12f. (e) For Zn (TOF = 12.5 h^{-1}): Mimoun, H. *J. Org. Chem.* **1999**, *64*, 2582−2589. (f) For Mo (TOF = 1.0 h^{-1}): Fernandes, A. C.; Romão, C. C. *J. Mol. Catal. A: Chem.* **2006**, *253*, 96−98. (g) For Ru (TOF = 33 h^{-1}, based on Ru): Matsubara, K.; Iura, T.; Maki, T.; Nagashima, H. *J. Org. Chem.* **2002**, *67*, 4985−4988. (h) For Rh (TOF = 16.7 h^{-1}): Ohta, T.; Kamiya, M.; Kusui, K.; Michibata, T.; Nobutomo, M.; Furukawa, I. *Tetrahedron Lett.* **1999**, *40*, 6963−6966. (i) For Pd (TOF = 2.8 h^{-1}): Nakanishi, J.; Tatamidani, H.; Fukumoto, Y.; Chatani, N. *Synlett* **2006**, *2006*, 869−872.

(27) Knijnenburg, Q.; Gambarotta, S.; Budzelaar, P. H. M. *Dalton Trans.* **2006**, 5442−5448.

(28) Mukhopadhyay, T. K.; MacLean, N. L.; Gan, L.; Ashley, D. C.; Groy, T. L.; Baik, M.-H.; Jones, A. K.; Trovitch, R. J. *Inorg. Chem.* **2015**, *54*, 4475−4482.

(29) Wang, M.; Weyhermüller, T.; Wieghardt, K. *Eur. J. Inorg. Chem.* **2015**, *2015*, 3246−3254.

(30) In our initial communication of **1**-mediated ketone and ester hydrosilylation (ref 25), it was proposed that catalysis takes place following electron transfer to the incoming substrate.

(31) Zhou, W.; Marquard, S. L.; Bezpalko, M. W.; Foxman, B. M.; Thomas, C. M. *Organometallics* **2013**, *32*, 1766−1772.

(32) Russell, S. K.; Bowman, A. C.; Lobkovsky, E.; Wieghardt, K.; Chirik, P. J. *Eur. J. Inorg. Chem.* **2012**, *2012*, 535−545.

(33) The phosphine co-donors of ^{Ph2PPr}PDI also dissociate during Mo-catalyzed aldehyde hydrosilylation, see: Pal, R.; Groy, T. L.; Bowman, A. C.; Trovitch, R. J. *Inorg. Chem.* **2014**, *53*, 9357−9365.

(34) PDI ligands are known to reversibly transfer two electrons to and from a first row metal during catalysis. For an early example, see: Bouwkamp, M. W.; Bowman, A. C.; Lobkovsky, E.; Chirik, P. J. *J. Am. Chem. Soc.* **2006**, *128*, 13340−13341.

(35) Cámpora, J.; Pérez, C. M.; Rodríguez-Delgado, A.; Naz, A. M.; Palma, P.; Álvarez, E. *Organometallics* **2007**, *26*, 1104−1107.

(36) Li, Y.; Li, Z.; Li, F.; Wang, Q.; Tao, F. *Tetrahedron Lett.* **2005**, *46*, 6159−6162.

(37) Ben-Daat, H.; Hall, G. B.; Groy, T. L.; Trovitch, R. J. *Eur. J. Inorg. Chem.* **2013**, *2013*, 4430−4442.

(38) Benkeser, R. A.; Landesman, H.; Foster, D. J. *J. Am. Chem. Soc.* **1952**, *74*, 648−650.

(39) Parr, R. G.; Yang, W. *Density Functional Theory of Atoms and Molecules*; Oxford University Press: New York, 1989.

(40) Bochevarov, A. D.; Harder, E.; Hughes, T. F.; Greenwood, J. R.; Braden, D. A.; Philipp, D. M.; Rinaldo, D.; Halls, M. D.; Zhang, J.; Friesner, R. A. *Int. J. Quantum Chem.* **2013**, *113*, 2110−2142.

(41) Perdew, J. P.; Burke, K.; Ernzerhof, M. *Phys. Rev. Lett.* **1996**, *77*, 3865−3868.

(42) Ditchfield, R.; Hehre, W. J.; Pople, J. A. *J. Chem. Phys.* **1971**, *54*, 724−728.

(43) Grimme, S.; Antony, J.; Ehrlich, S.; Krieg, H. *J. Chem. Phys.* **2010**, *132*, 154104.

(44) Dunning, T. H., Jr. *J. Chem. Phys.* **1989**, *90*, 1007−1023.

(45) (a) Marten, B.; Kim, K.; Cortis, C.; Friesner, R. A.; Murphy, R. B.; Ringnalda, M. N.; Sitkoff, D.; Honig, B. *J. Phys. Chem.* **1996**, *100*, 11775−11788. (b) Edinger, S. R.; Cortis, C.; Shenkin, P. S.; Friesner,

DOI: 10.1021/jacs.7b00879
J. Am. Chem. Soc. 2017, 139, 4901−4915

R. A. *J. Phys. Chem. B* **1997**, *101*, 1190−1197. (c) Friedrichs, M.; Zhou, R.; Edinger, S. R.; Friesner, R. A. *J. Phys. Chem. B* **1999**, *103*, 3057−3061.
(46) Noodleman, L. *J. Chem. Phys.* **1981**, *74*, 5737−5743.

DOI: 10.1021/jacs.7b00879
J. Am. Chem. Soc. 2017, 139, 4901−4915